Accepted Manuscript

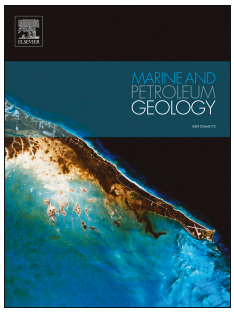

Permeability evolution across carbonate hosted normal fault zones

Thomas J. Haines, Emma A.H. Michie, Joyce E. Neilson, David Healy

PII: S0264-8172(16)30008-3

DOI: 10.1016/j.marpetgeo.2016.01.008

Reference: JMPG 2438

To appear in: *Marine and Petroleum Geology*

Received Date: 19 May 2015

Revised Date: 27 December 2015

Accepted Date: 10 January 2016

Please cite this article as: Haines, T.J., Michie, E.A.H., Neilson, J.E., Healy, D., Permeability evolution across carbonate hosted normal fault zones, *Marine and Petroleum Geology* (2016), doi: 10.1016/j.marpetgeo.2016.01.008.

Title

Permeability evolution across carbonate hosted normal fault zones

Authors and Addresses

Thomas J. Haines[1,2]

Emma A. H. Michie[1,3]

Joyce E. Neilson[1]

David Healy[1]

[1] School of Geosciences, King's College, University of Aberdeen, Aberdeen AB24 3UE, UK

[2] Badley Ashton and Associates Ltd, Winceby House, Winceby, Horncastle, Lincolnshire LN9 6PB, UK

[3] Badley Geoscience Ltd, North Beck House, North Beck Lane, Hundleby, Lincolnshire PE23 5NB, UK

Corresponding author

Thomas J. Haines,

Email: tj.haines.88@gmail.com

Telephone: +447917692228,

Correspondence/ present address: Badley Ashton and Associates Ltd, Winceby House, Winceby, Horncastle, Lincolnshire LN9 6PB, UK

Abstract

Carbonate lithologies tend to have highly heterogeneous and tortuous pore systems that are created and/ or modified by diagenetic and tectonic processes following deposition. The correlation between porosity and permeability in carbonate lithologies is often poor as a result of their heterogeneous and complex pore systems. To effectively predict permeability, it is necessary to understand the processes that modify pore systems and quantify the impact of these modifications on permeability. Using outcrop exposures of normal fault zones hosted in carbonate lithologies on the Maltese Islands, this study documents the evolution of textures in contrasting carbonate lithofacies (wackestones, packstones and pack/grainstones) across two normal fault zones of varying displacement (*c*. 10 and 100 m). The pore system modifications associated with these textural changes are quantified using image analysis and point count methods, while porosity and permeability are measured across the studied fault zones using core plug porosimetry and permeametry techniques.

The fault related processes that occur within the fault zones are controlled by the primary lithofacies and to a lesser extent the fault displacement. Aggrading neomorphism is observed within the damage zones in the grain supported lithofacies and is postdated by fracturing. In the micrite supported lithofacies in the same damage zones, aggrading neomorphism is absent, but fracturing is prevalent. In the fault core, brecciation occurs in both lithofacies within the 10 and 100 m displacement fault zones, while cataclasis is only active in the grain supported lithofacies in the higher displacement fault zone. The mineralogical and textural compositions of the primary lithofacies dictate the processes that occur in the fault zones. These processes variably modify the pore systems and hence control the temporal evolution of permeability in the fault zones. Such observations can help understand reservoir quality distribution around fault zones in the subsurface reservoirs.

Keywords

permeability; porosity; pore systems; carbonates; normal fault zones

1 Introduction

Pore systems control the permeability of rocks. In carbonate lithologies, the pore systems reflect the depositional processes that form the rock and the diagenetic and tectonic processes that modify it. Immediately following deposition, permeability is higher in grainstones compared to packstones and wackestones because the grainstones contain larger quantities of connected interparticle macropores, while the packstones and wackestones host less macropores and are typically dominated by micropores due to the occurrence of lime mud (Loucks, 2002; Lucia, 1995). Additionally, the permeability in grainstones tends to increase with increasing grain sizes and better sorting (Lucia, 1995). Hydrodynamism controls on the quantity of lime mud, the grain size and the sorting and is hence a key depositional control on permeability (Loucks, 2002). Melim et al. (2001) shows that intraparticle macropores, such as those hosted within foraminifera, do not significantly contribute to permeability due to their isolated distribution. This indicates that the environmental conditions that promote the development of a given faunal assemblage, such as light and turbidity, also impose a depositional control on permeability.

Due to their metastable mineralogical compositions, carbonate lithologies are prone to significant diagenetic modifications following deposition. These textural changes can significantly modify the pore systems and drastically change the permeability. For example, calcite cementation has locally and pervasively occluded the primary interparticle macropore volume in shoal and marginal shoal deposits in the Natih E Member in Oman (Hollis et al., 2010). As a result of this calcite cementation, the average permeability decreases from 15.5mD to 2.84mD (Hollis et al., 2010). In similar shoal deposits in the Natih A and C

Members, non-fabric selective leaching of the skeletal allochems has created abundant vugs and moulds; the pore system created by this dissolution has an average permeability of 324mD (Hollis et al., 2010).

In addition to diagenesis, tectonic stresses can overprint carbonate textures, modify the pore systems and ultimately impact the permeability. At the field to basin-scale, tectonic stresses can create a range of different structures including normal fault zones and fold and thrust belts. This study uses outcrop exposures to understand the impact of normal faulting on the evolution of permeability in carbonate lithologies. Normal fault zones are traditionally characterised into architectural elements (e.g. Caine et al., 1996; Agosta and Aydin, 2006; Mitchell and Faulkner, 2009). Caine et al. (1996; and references therein) proposed a simple model that categorises fault zones into a damage zone and a fault core. Damage zones are networks of subsidiary fault related structures, including small faults, veins, fractures, cleavage and folds (Caine et al., 1996). Alternatively, they are defined as the areas surrounding a fault in which the fracture density is above the background regional fracture density due to the presence of fault related structural elements that are absent elsewhere (Agosta and Aydin, 2006). Damage zones can be subdivided into different architectural elements based on the abundance and/or connectivity of structural features, such as fractures (Agosta and Aydin, 2006; Micarelli et al., 2006). For example, Micarelli et al. (2006) subdivide damage zones into intensely deformed (IDDZ) and a weakly deformed (WDDZ) according to the density and connectivity of fractures. The fault core can be composed of single or multiple slip surfaces and a range of different fault lithologies, such as carbonate breccias, carbonate cataclasites, carbonate and shale gouges, secondary calcite cements, veins and host rock lenses (Bastesen and Braathen, 2010; Chester and Logan, 1987; Mitchell and Faulkner, 2009; Sibson, 1977). The types of deformation that occur within fault zones are a function of porosity and primary lithofacies texture (Fossen et al., 2007; Underhill and

Woodcock, 1987). For example, fractures form in low porosity carbonates in the damage zone of the Venere Fault Zone (Agosta et al., 2007), while in high porosity grainstones deformation bands develop as a result of grain rotation, compaction and cataclasis (Rath et al., 2011). Due to the creation of connected fracture networks, damage zones tend to have enhanced permeability relative to the protolithology (Agosta et al., 2010; Caine et al., 1996; Chester and Logan, 1986; Larsen et al., 2010). For example, the creation of fractures in low porosity carbonates in the Venere Fault Zone results in an increase in permeability relative to the protolithology (Agosta et al., 2007). In the fault core, cataclasis can cause pore systems to collapse resulting in permeability decreases (Micarelli et al., 2006; Tondi, 2007). Rath et al. (2011) document porosity reductions of 20 to 30 % and permeability decreases of 3 orders of magnitude, compared to protoliths, as a result of grain rotation, compaction and cataclasis in grainstones from the Eisenstadt-Sopron Basin (Austria and Hungary).

Due to diagenetic and deformation processes, carbonate lithologies have highly heterogeneous and tortuous pore systems, which result in complicated porosity-permeability relationships and a poor understanding of the controls on permeability (Hollis et al., 2010; van der Land et al., 2013). A key approach to understanding permeability in carbonates is to document pore system characteristics (Anselmetti and Eberli, 1999; Budd, 2002; Melim et al., 2001; van der Land et al., 2013). For example, Budd (2002) documents textural and pore system modifications associated with cementation and compaction in carbonate grainstones to understand the evolution of permeability. However, no studies have quantified the evolution of pore systems according to fault damage and the associated diagenesis in carbonate lithologies. This study characterises textural changes and the resultant pore system modifications across outcrop exposures of two carbonate hosted normal fault zones on the Maltese Islands to understand the spatial and temporal evolution of permeability in carbonate

lithologies according to fault damage and fault related diagenesis. Such an understanding can be applied to subsurface reservoirs to improve reservoir quality predictions.

2 Geological Background

2.1 Stratigraphy

The Maltese Islands, which are located in the central Mediterranean (Figure 1 a and b), are composed of a sequence of Oligo-Miocene shallow water to pelagic carbonates (Buxton and Pedley, 1989). The stratigraphy of the Maltese Islands is subdivided into four Formations (Pedley et al., 1976) (Figure 1 c). This study focusses on the two lowermost exposed Formations: the Oligocene Lower Coralline Limestone Formation and the Miocene Globigerina Limestone Formation (Figure 1 c). The Lower Coralline Limestone Formation is subdivided into four Members, which are, from oldest to youngest: 1) Il Maghlaq (Lcm), 2) Attard (Lca), 3) Xlendi (Lcx) and 4) Il Mara (Lcim) Members (Pedley, 1978) (Figure 1 c). The Lower Coralline Limestone Formation is dominantly composed of coralline algae and larger benthic foraminifera rich wackestones, packstones, pack/grainstones, grainstones, floatstones and rudstones. The Globigerina Limestone Formation is subdivided into three members (Pedley et al., 1976), which are separated by hardground-conglomerate couplets and include (from oldest to youngest) 1) Lower Globigerina (Lgl), 2) Middle Globigerina (Mgl) and 3) Upper Globigerina Limestone (Ugl) Members (Pedley et al., 1976) (Figure 1 c). Bryozoa wackestones and packstones and planktonic foraminiferal lime mudstones and wackestones comprise the Globigerina Limestone Formation.

2.2 Normal Fault Zones

The carbonates of the Maltese Islands are dissected by normal fault zones, which trend either ENE-WSW or NW-SE and range in displacement from several centimetres to greater than 100 m. The normal fault zones are associated with the Pantelleria, Linosa and Malta Grabens,

which formed due to crustal extension in the foreland of the Maghrebian-Apennine fold and thrust belt (Figure 1 a), possibly related to either ridge-push/ slab-pull and or pull-apart kinematics (Gatt, 2012). Major fault activity occurred from the Late Miocene onwards and, despite the differing fault trends, it is thought to be caused by a single phase of deformation (Dart et al., 1993).

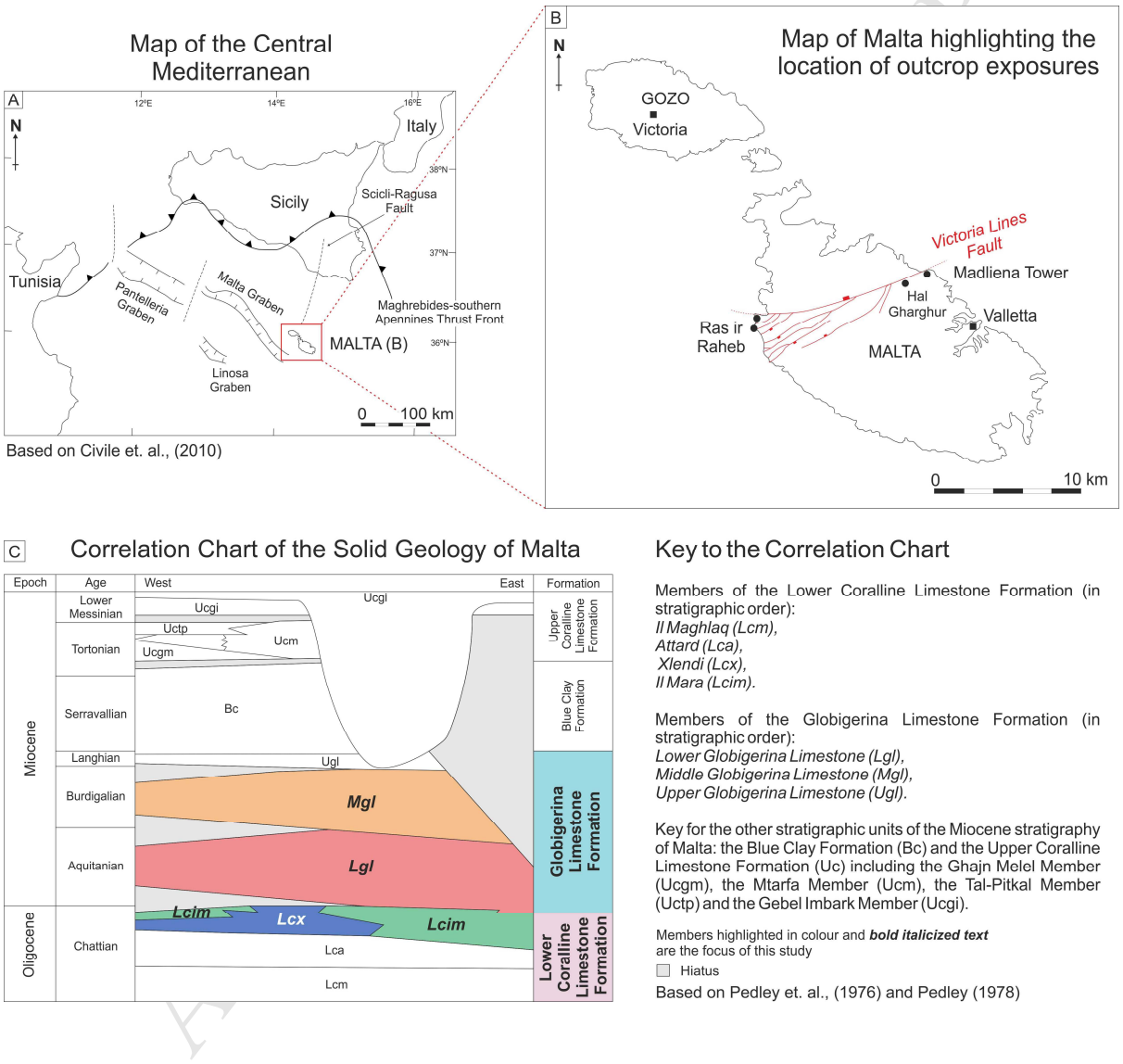

Figure 1 - A) Simplified tectonic map of the central Mediterranean region highlighting the location of the Maltese Islands (based on Civile et al., 2010). B) Map of the Maltese Islands displaying the location of the Ras ir Raheb Fault Zone and the Victoria Lines Fault Zone. The black filled circles display the field localities used in this study. C) Correlation chart displaying the Oligo-Miocene lithostratigraphy of the Maltese Islands (based on Pedley et al. (1976) and Pedley (1978)).

This study focusses on two normal fault zones that dissect the Oligo-Miocene carbonates: 1) the Ras ir Raheb Fault Zone, which is an 11.7 m displacement fault zone exposed on the western coast of Malta at Ras ir Raheb (Figure 1 b) and 2) the Victoria Lines Fault Zone, which is a c. 100 m displacement fault zone (Pedley et al., 1976), that crops out across Malta, but is particulary well exposed on the northeast coast at Madliena Tower (Figure 1 b). Michie et al. (2014) classify the fault zones into architectural elements including the protolith, which is undeformed and displays no fault related diagenesis, the weakly deformed damage zone (WDDZ), the fracture splay zone (also known as the intensely deformed damage zone, IDDZ) and the fault core. The WDDZ presents elevated fracture intensities and densities compared to the protolith, while the the fracture splay zone, which is positioned within the hanging wall (HW), is bound by fault surfaces and is characterised by the highest fracture intensities and densities within the fault zone (Michie et al., 2014). The fault core, which is distributed along slip surfaces, is the zone where the majority of the fault deformation is accommodated; the fault core incorporates fault lithologies such as breccias, cataclasites and gouges (Michie, 2015).

3 Methodology

3.1 Sample Database

67 oriented rock samples were collected across the HW, principal slip surface (PSS) and the footwall (FW) of the Ras ir Raheb (34) and Victoria Lines (33) fault zones. HW samples are henceforth annotated as negative distances from the PSS, whereas positive distances represent FW samples.

The rock samples were collected at semi-regular intervals away from the PSS in selected horizons in the Lower Coralline Limestone and Globigerina Limestone Formations in contrasting lithofacies. The sampling included the complete range of architectural elements

(e.g. Michie et al., 2014) and fault textures in the fault zones. As a result of weathering patterns on cliff faces and a lack of suitable exposure, the sampling was not conducted at regular intervals away from the PSS. 140 core plugs were prepared from the 67 rock samples to conduct petrophysical analyses. Multiple core plugs were taken from the same rock sample where possible to assess the sample heterogeneity.

3.1.1 Sample Subset

A subset of 29 rock samples was selected from the complete sample database for petrographic analyses and pore system characterisation using image and point count methodologies. The subset included 14 samples from the Ras ir Raheb Fault Zone, 13 samples from the Victoria Lines Fault Zone and 2 additional undamaged samples. The subset samples incorporated all architectural elements within the two fault zones, as well as all the observed fault textures.

A total of 87 thin sections were prepared from the sample subset, including three orthogonal thin sections per sample (for the 29 samples in the subset). Orthogonal thin sections were prepared to assess textural heterogeneity and pore system anisotropy and heterogeneity.

3.2 Field Survey

Sedimentary logging techniques were used to characterise the protolith lithofacies, while geological mapping techniques were used by Michie et al. (2014) to define the architectural elements and hence fault architecture in the two fault zones. Fracture analysis was conducted at regular intervals perpendicular to the strike of each fault zone to characterise fracture patterns, in particular the variation in fracture density. Fracture density is the mean number of fractures per unit area; fracture density was calculated using a circular scanline approach by counting the number of fracture endpoints in a circular window of a given area (Mauldon et al., 2001).

3.3 Petrographic Analysis

In order to understand the fault damage and diagenetic processes that have occurred in the two fault zones, as well as their relative timing, petrographic analysis under transmitted-light was undertaken on the 87 thin sections corresponding to the 29 samples in the subset. The thin-sections were prepared to a standard size (3" by 1") and thickness (30µm) and were impregnated with blue-dyed epoxy resin to qualitatively characterise the pore systems.

3.4 Petrophysical Analysis

3.4.1 Helium Porosimetry

A Coberly-Stevens porosimeter was used to quantify He-porosity on the 140 core plugs corresponding to the 67 rock samples in the complete sample database. The core plugs were 1" in diameter and varied in length typically between 1 and 2"; the short core plug lengths (i.e. 1") resulted from the breakage of core plugs due to relatively poor cohesion, notably within the Globigerina Limestone Formation.

He-porosity was derived from the grain volume, V_g, and the bulk volume, V_b, of the core plug (Equation 1). The grain volume was calculated by injecting a known helium volume at a given pressure into the core plug and applying Boyle's Law, which states that, at a constant temperature, the pressure of a given amount of gas will increase as the volume that the gas occupies decreases. The bulk volume was calculated by measuring the dimensions of the core plug.

Equation 1

$$\phi\ (\%) = \frac{V_b - V_g}{V_b} \times 100$$

The He-porosity measurement was repeated three times for each core plug. The standard deviation was then calculated to assess the experimental error; where the standard deviation

revealed a high degree of variability between the repeated porosity measurements, the porosity was repeated to validate the accuracy. The He-porosity value quoted in this study is the arithmetic mean of the three porosity measurements.

3.4.2 Nitrogen Permeametry

A Jones Nitrogen Permeameter was used to quantify steady-state permeabilities on the same 140 core plugs in which He-porosity was measured. These core plugs correspond to the 67 rock samples comprising the complete sample database.

3.4.2.1 Permeability Calculation: Darcy's Law

According to Darcy's Law (equation 2), the permeability (k) of a rock is a function of the flow rate (q), the fluid viscosity (μ) (0.0176 cP for N_2 at room temperature), the cross sectional area (a) and the pressure drop (P_{in} - P_{out}) over a given flow length (l). Steady-state permeabilities were calculated by measuring the flow rate of nitrogen through the core plugs using a Jones Nitrogen Permeameter at ambient temperature and pressure. Flow rates were measured by two techniques depending on their magnitude. The built-in flowmeter technique was used to measure flow rates of greater than 0.025 ml/s, while the travelling meniscus flowmeter was used to measure flow rates of less than 0.025 ml/s and greater than 0.0001 ml/s. The measured flow rate was applied to Darcy's Law to calculate the core plug permeability (Equation 2). This technique accurately measures permeabilities as low as c. 0.0001mD.

Equation 2

$$k\,(mD) = \frac{2 \times q \times \mu \times (l/a)}{P_{in}^{2} - P_{out}^{2}}$$

Gas slippage on the pore walls can increase gas permeametry measured permeability compared to the true permeability of other fluids, such as oil (Klinkenberg, 1941; Tanikawa

and Shimamoto, 2006). To address gas slippage effects, the Klinkenberg correction was applied to the calculated permeabilities.

3.5 Pore System Characterisation

3.5.1 Image Analysis

3.5.1.1 Workflow

Image analysis of backscatter electron (BSE)-SEM photomicrographs was used to quantify pore sizes in 29 subsetted samples using the methodology outlined in Haines et al. (2015).

Photomicrographs were systematically acquired with identical brightness and contrast values. The selected brightness and contrast values both accurately represented the pore system and provided a significant level of contrast between the phases of interest (porosity and rock). A minimum of six BSE-SEM images of equal magnification were acquired and stitched together to create pore system images. This approach enabled the imaging of pores with diameters ranging from less than 0.5 µm to greater than 1000 µm. Three different pore system images were collected for each thin section (bottom, centre and top). The image acquisition workflow was repeated on perpendicularly oriented thin sections in each sample to allow the quantification of pore sizes in three dimensions. Consequently, the pore sizes in each sample were quantified from nine pore system images, comprising a minimum of 54 individual BSE-SEM photomicrographs. This number is consistent with the quoted number of 15 to 30 fields of view required for representative image analysis porosity quantification (Ehrlich et al., 1991; Solymar and Fabricius, 1999).

The pore system images were composed of greyscale pixels, which were subdivided into two phases: 1) the pore phase, represented by black greyscale values and 2) the rock phase, represented by any greyscale value except those that correspond to black. Using image

analysis software (ImageJ), the greyscale pore system images were converted into binary images of the rock and pore phases by systematic thresholding. Pores intersecting the edges of the binary pore system images were removed because such pores incompletely represented the field of view and provided artefact pore sizes.

3.5.1.2 Pore Size Descriptors

Using ImageJ, pore sizes can be measured by a variety of different descriptors such as the Feret diameter or the major axis of a fit ellipse (Rasband, 2014). This study used the Feret diameter pore size descriptor to describe pore sizes. The Feret diameter of a pore is the longest distance between any two points on the pore boundary. It is measured by rotating the pore 360 ° around its centre point and measuring the distance between the pore boundary at 0 and 180 ° for each step of the rotation; the Feret diameter is the largest measured distance.

In this study, pore sizes were subdivided into three classes: micro, meso and macro pore sizes. The micro pore size class includes all pores with a Feret diameter of less than 10 µm. The meso pore size class includes all pores with a Feret diameter between 10 and 100 µm and the macro pore size class includes all pores with a Feret diameter of greater than 100 µm. The fraction of each pore size class comprising a sample is multiplied by the average He-porosity in the corresponding sample to quantify the amount of porosity associated with each pore size class.

3.5.2 Point Count Analysis

Point count analysis was used to quantify pore types in 29 subsetted samples The point count methodology employed in this study utilized high resolution optical photomicrographs of full thin sections to systematically count pore types. The thin sections used for the point count analysis correspond to the same thin sections used in the petrographic and image analysis and to the same samples from which petrophysical analyses were conducted. The optical

photomicrographs were fixed to equal dimensions and resolution. A square mesh of dashed lines of equal dimensions was centred over the top of each full thin optical photomicrograph. Every pore that intersected the mesh was counted and weighted according to the number of dashes intersecting its length. In the majority of instances, this methodology counted in excess of 300 points, which is in line with the quoted number of points (250 - 300) required for statistically significant results (Tucker et al., 1988). In the instances where less than 300 points were counted, the porosity tended to be very low. To increase the statistical significant in such instances, multiple thin sections from the same sample were analysed. Similarly, if significant textural heterogeneity was apparent between different thin sections in the same sample, multiple thin sections were analysed. The data is presented as dominant pore types; dominant pore types are defined as those with the highest occurrence in a sample.

3.5.2.1 Pore Type Terminology

Pore types were classified according to porosity classification systems of Lønøy (2006) and Choquette and Pray (1970). Pore types were subdivided into eight categories according to sedimentological, diagenetic and damage textural characteristics. The categories included intergranular, intragranular, intercrystalline, mudstone microporosity (matrix), mouldic, vuggy, fracture and breccia (Choquette and Pray, 1970; Lønøy, 2006). For the purposes of this study, mudstone micro pore types of Lønøy (2006) are re-named as matrix pore types to avoid confusion with the image analysis derived pore size data. Matrix pore types are defined as pore types which are too small to be accurately characterised by point counting techniques but are visible under optical microscopy. All other pore types definitions used in this study are identical to those of previous pore type classifications (Choquette and Pray, 1970; Lønøy, 2006).

4 Results

4.1 Protoliths

Lithologies that have neither experienced fault damage nor fault related diagenesis are defined as protoliths in this study. To understand the impact of fault damage and fault related diagenesis on permeability, it is necessary to first characterise the depositional and diagenetic textures of the protoliths.

4.1.1 Depositional Textures

Two contrasting protoliths are tracked across the HW, PSS and FW of the Ras ir Raheb Fault Zone; these protoliths correspond to stratigraphic horizons within the Il Mara Member (Lcim) of the Lower Coralline Limestone Formation and the Middle Globigerina Limestone Member (Mgl) of the Globigerina Limestone Formation (Figure 1 c).

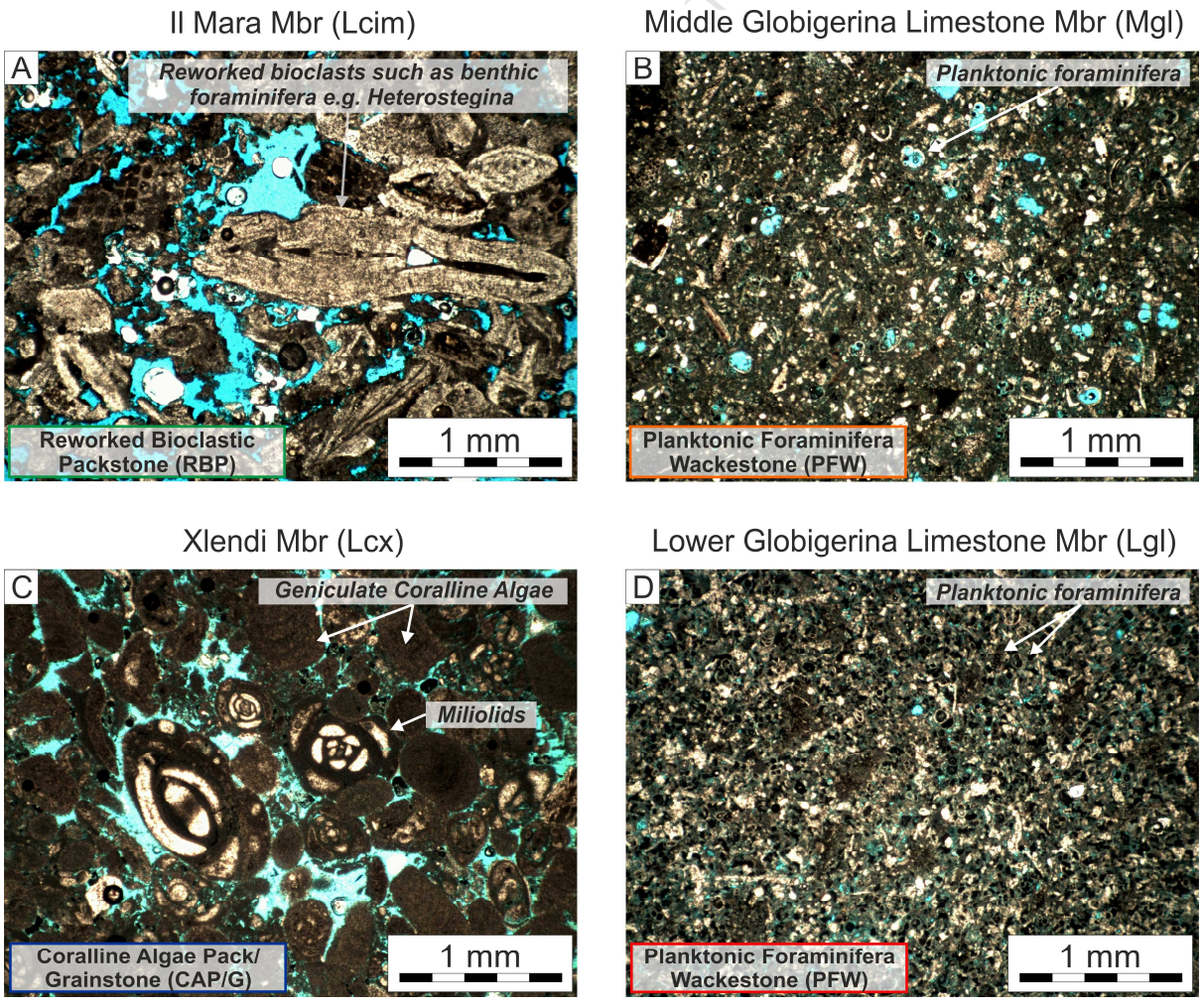

Figure 2 - Optical photomicrographs (PPL) of the protoliths studied in the Ras ir Raheb and Victoria Lines fault zones. Ras ir Raheb Fault Zone: A) the reworked bioclastic packstone (RBP) lithofacies in the Lcim (see Figure 1 c) and B) the planktonic foraminifera wackestone (PFW) lithofacies in the Mgl. Victoria Lines Fault Zone: C) the coralline algae packstone/grainstone (CAP/G) lithofacies in the Lcx and D) the planktonic foraminifera wackestone (PFW) lithofacies in the Lgl.

The stratigraphic horizon studied in the Lcim is a reworked bioclastic packstone (RBP) comprising heavily reworked larger benthic foraminifera, such as *Lepidocyclina*, and bryozoa in a micritic matrix (Figure 2 a). In the Mgl, the studied stratigraphic horizon consists of a planktonic foraminifera wackestone (PFW) with *Globigerina* and fine bioclastic debris in a micritic matrix (Figure 2 b).

Similarly, two contrasting protoliths are tracked across the Victoria Lines Fault Zone corresponding to stratigraphic horizons in the Xlendi Member (Lcx) of the Lower Coralline Limestone and the Lower Globigerina Limestone Member (Lgl) of the Globigerina Limestone Formation. The stratigraphic horizons are only tracked across the FW or HW of this fault zone and not both due to the limited outcrop exposure. The studied stratigraphic horizon in the FW, which is a pack-grainstone composed of geniculate coralline algae and miliolids (Figure 2 c), corresponds to the Lcx. This lithofacies is termed the coralline algae pack/grainstone (CAP/G). In the HW, the studied stratigraphic horizon corresponds to a wackestone consisting of planktonic foraminifera and fine bioclastic debris in a micritic matrix (Figure 2 d). This lithofacies unit is termed the planktonic foraminifera wackestone (PFW), however, unlike in the Ras ir Raheb Fault Zone, this lithofacies corresponds to the Lgl rather than the overlying Mgl (Figure 1 c).

4.1.2 Diagenetic Modifications

The diagenetic modifications that occur directly or indirectly as a response to faulting can only be differentiated from those diagenetic processes that occur prior to faulting by

documenting the diagenetic history of the protoliths. Across the Maltese Islands, the diagenetic alteration of the Lower Coralline Limestone and Globigerina Limestone Formations is limited by shallow burial of the sediments (up to 300 m; Bonson et al., 2007).

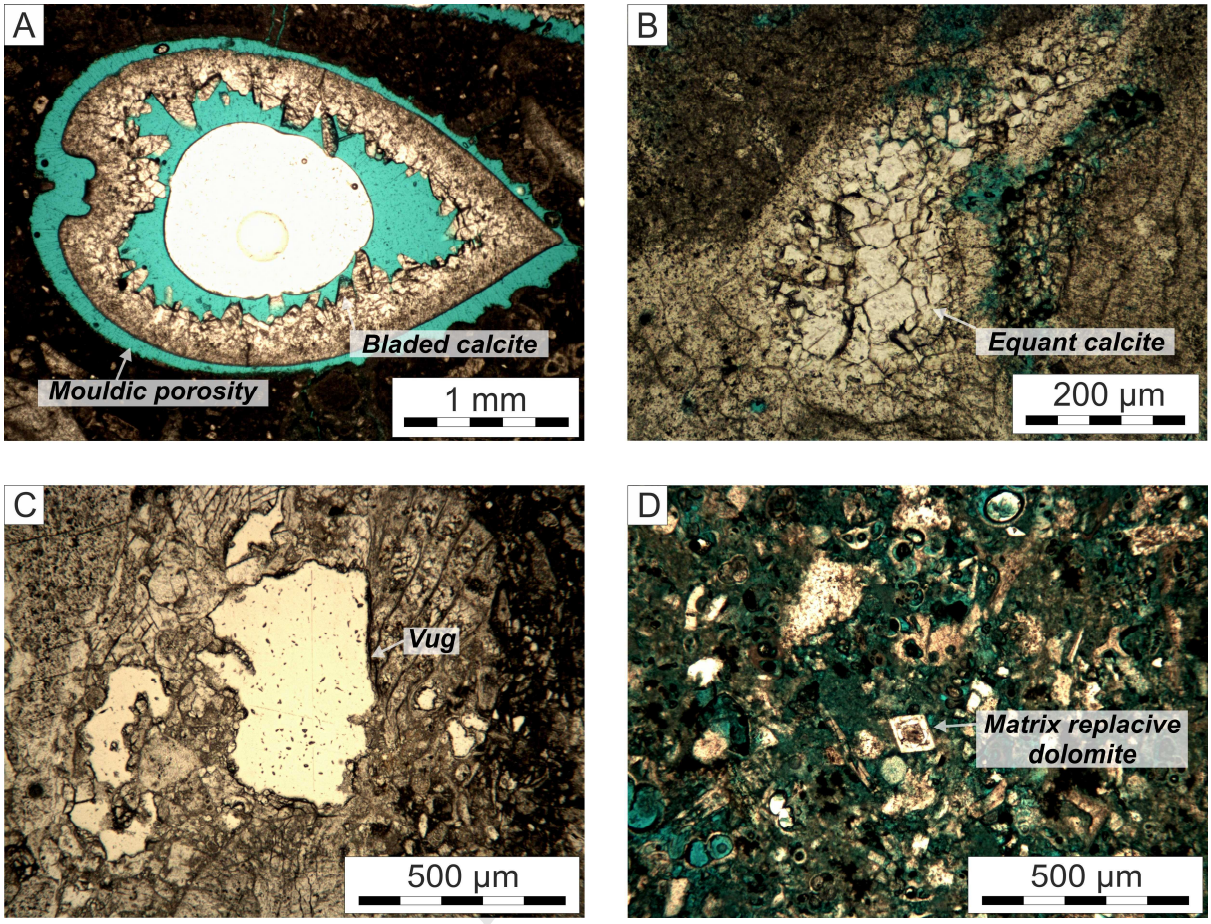

Figure 3 - Optical photomicrographs (PPL) of the dominant diagenetic phases that occurred prior to faulting within the protoliths. A) Bladed calcite cement and mouldic porosity created by the first phase of fabric selective dissolution. B) Equant calcite cement. C) A vug formed by non-fabric selective dissolution. D) Matrix replacive dolomite.

The diagenesis is dominantly characterised by minor calcite cementation and minor dissolution (Figures 3 a-c), however, very rare early replacive dolomite is also observed in the Mgl only (e.g. PFW lithofacies; Figure 3 d).

Fault Zone	Location	Formation	Member	Lithofacies unit	Notation
Ras ir Raheb Fault Zone (displacement = 11.7 m)	HW and FW	Globigerina Limestone	Middle Globigerina Limestone (Mgl)	Planktonic Foraminifera Wackestones	PFW
	HW and FW	Lower Coralline Limestone	Il Mara (Lcim)	Reworked Bioclastic Packstones	RBP
Victoria Lines Fault Zone (displacement = c. 100 m)	HW	Globigerina Limestone	Lower Globigerina Limestone (Lgl)	Planktonic Foraminifera Wackestones	PFW
	FW	Lower Coralline Limestone	Xlendi (Lcx)	Coralline Algae Pack/ Grainstones	CAP/G

Table 1 - Summary of the lithofacies units and corresponding stratigraphic horizons (see Figure 1 c) tracked across the Ras ir Raheb and Victoria Lines fault zones.

Three minor phases of calcite cementation are defined based on their crystal habit: 1) fibrous, 2) bladed (Figure 3 a) and 3) equant (Figure 3 b); the three phases have been linked to marine, meteoric and shallow marine burial fluids respectively (Knoerich and Mutti, 2006) and are both pore lining (Figure 3 a and b) and syntaxial on echinoderm fragments. Three separate phases of minor dissolution have also been identified (Figure 3 a and c). The first two phases of dissolution are fabric selective and have created mouldic pores (Figure 3 a). These dissolution phases are particularly prevalent in those stratigraphic units that contain susceptible aragonitic skeletal fragments, such as the Lcim (e.g. RBP lithofacies; Figure 3 a). The final dissolution phase is non-fabric selective and has created vugs (Figure 3 c). This dissolution phase, which is the most volumetrically significant, is likely to be occurring in the modern meteoric environment.

The different calcite cement and dissolution phases are subtly more volumetric in the grain supported lithofacies in the Lower Coralline Limestone Formation (e.g. the RBP and CAP/G lithofacies) compared to the micrite supported lithofacies in the Globigerina Limestone Formation (e.g. PFW lithofacies).

4.2 Ras ir Raheb Fault Zone

This section and the following section (*4.3 Victoria Lines Fault Zone*) describe the architecture, as well as the field and microscale fault related deformation and diagenesis in the two fault zones. Porosity and permeability are linked to the architectural elements, while pore systems changes across the fault zones are outlined.

4.2.1 Fault Architecture

The Ras ir Raheb Fault Zone is subdivided into three architectural elements: 1) the fault core, 2) the fracture splay zone and 3) the weakly deformed damage zone (WDDZ) (Michie et al., 2014).

The fault core is characterised by discontinuous lenses of breccia, which are located adjacent to the PSS on the HW side only (Figure 4). The breccia lenses are up to 0.6 m in thickness and originate from the RBP (Figure 4 b) and the PFW lithofacies (Figure 4 c), however, larger quantities of breccia have developed in the RBP lithofacies. Mosaic breccias (*cf.* Woodcock and Mort, 2008), which originate from the RBP lithofacies and are composed of *c.* 65 % breccia clasts, have developed in the discontinuous lenses (Figure 5). The discontinuous breccia lenses in the PFW lithofacies were not sampled successfully in this study.

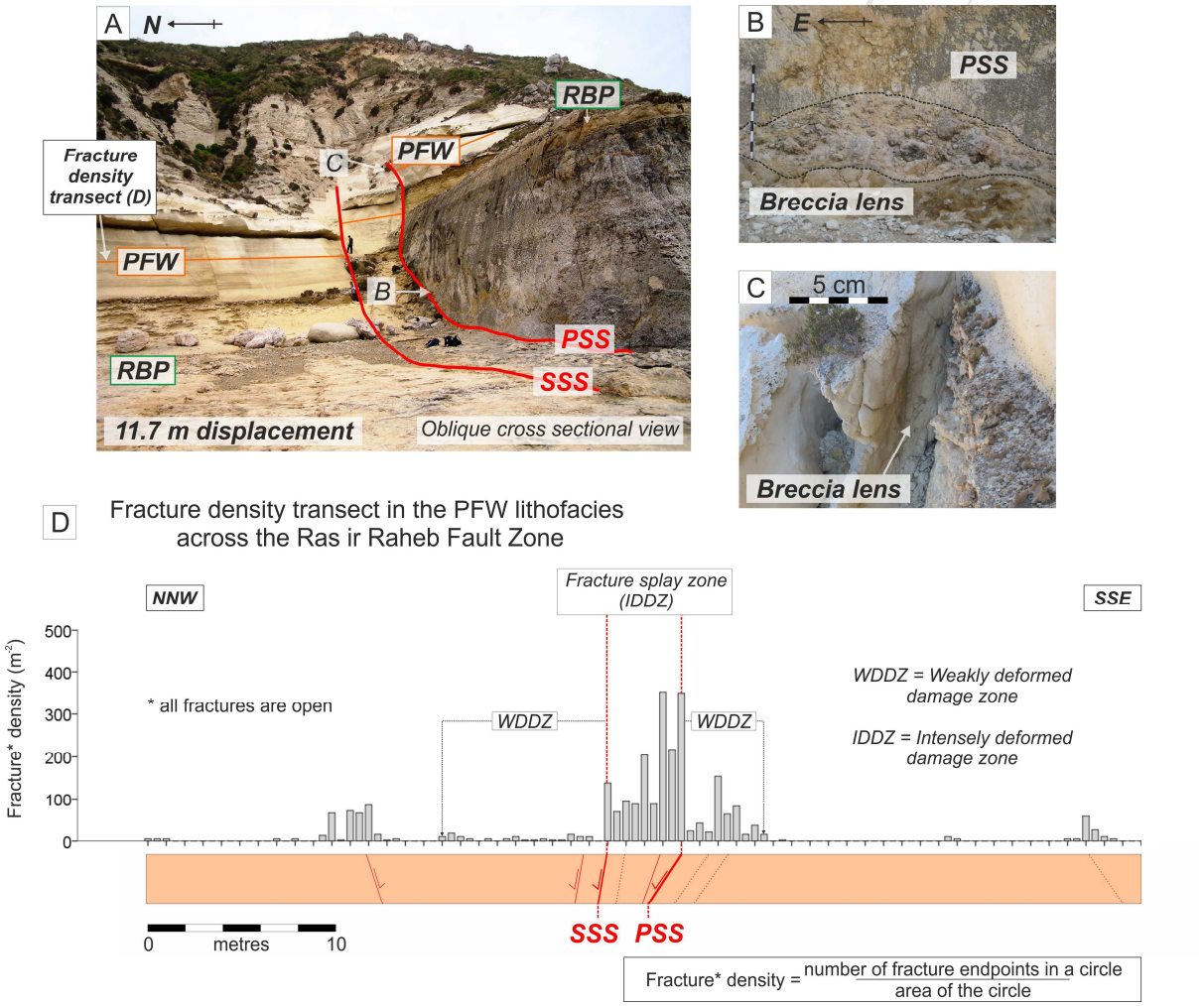

Figure 4 - An overview of the fault architecture in the Ras ir Raheb Fault Zone. A) A field photograph of the Ras ir Raheb Fault Zone, highlighting the slip surfaces and the studied lithofacies. Field photographs of breccia lenses in B) the RBP lithofacies and C) PFW lithofacies. D) A fracture density transect across the fault zone in the PFW lithofacies displaying the fault

architecture. The positions of the breccia lenses photographs and the fracture density transect are displayed in A.

Open fractures observed within the fracture splay zone and WDDZ. The fracture splay zone, which is located within the HW only and is bound by the PSS and a subsidiary slip surface (SSS), displays fracture densities greater than 100 m^{-2}; (Figure 4 a and d). The fracture splay zone is developed in both the RBP and the PFW lithofacies and is 5-6 m wide in this fault zone (Figure 4 d). The WDDZ is observed within the HW and FW of the fault zone surrounding the fracture splay zone; the fracture densities in the WDDZ are typically 100 m^{-2} or less (Figure 4 d).

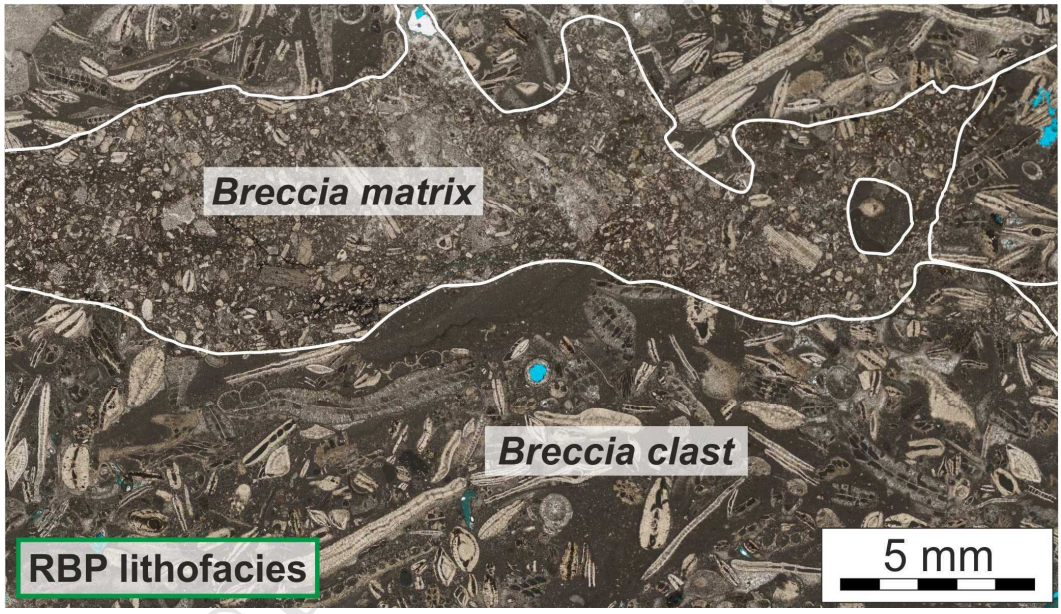

Figure 5 - Optical photomicrograph (PPL) of a mosaic breccia that is found within lenses on the PSS; this breccia originates from the RBP lithofacies.

4.2.2 Porosity and Permeability

Porosity and permeability are subdivided according to the lithofacies and the fault architectural element in the Ras ir Raheb Fault Zone (Figure 6). In the RBP lithofacies, the protolith porosity ranges from 9 to 23%, while the permeability varies from less than 0.01mD to 200mD (Figure 5 a; green shading). In the fault zone, the porosity and permeability in this

lithofacies are either comparable or are less than the protolithology; porosity is typically 10% (Figure 6 a). The porosity is particularly low in the brecciated fault core, i.e. less than 4 %, while in the fracture splay zone and WDDZ, the porosity ranges from 3 to 14%. The permeability in the fault zone can exceed 10mD, however, it is typically less than 0.01mD (Figure 6 a). Additionally, there are no clear permeability trends according to the fault architectural element. In the PFW protolithology, porosity ranges from 26-36 % and permeability is between 0.1 and 2mD (Figure 6 b; red shading). In the fracture splay zone and WDDZ, the porosity and permeability are comparable or are subtly less than the protolithology range, while in the fault core, porosity can be reduced to 6 % and permeability to 0.004mD (Figure 6 b).

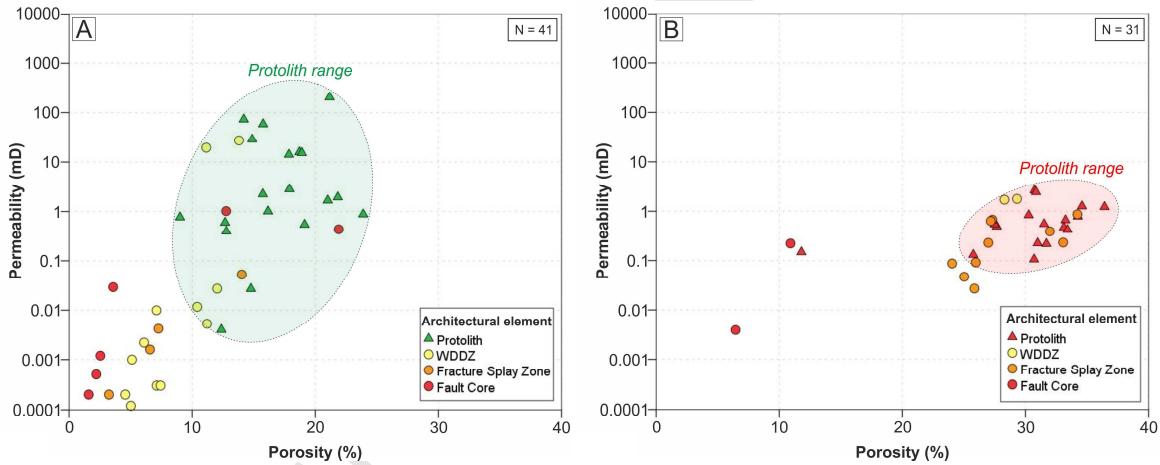

Figure 6 - Cross plots of porosity-permeability subdivided according to the protolith lithofacies and the fault architectural elements in the Ras ir Raheb Fault Zone: A) RBP lithofacies and B) PFW lithofacies.

4.2.3 Fault Related Diagenesis

In the RBP lithofacies, cryptocrystalline to finely crystalline calcite cements replace the primary micrite and bioclastic fragments, such as bryozoa, in the fault core, fracture splay zone and the WDDZ, up to distances of 12 m from the PSS (Figure 7 a and b). The cryptocrystalline to finely crystalline calcite has irregular, curved and embayed

intercrystalline boundaries (Figure 7 b), which are indicative of neomorphic cements (Bathurst, 1975).

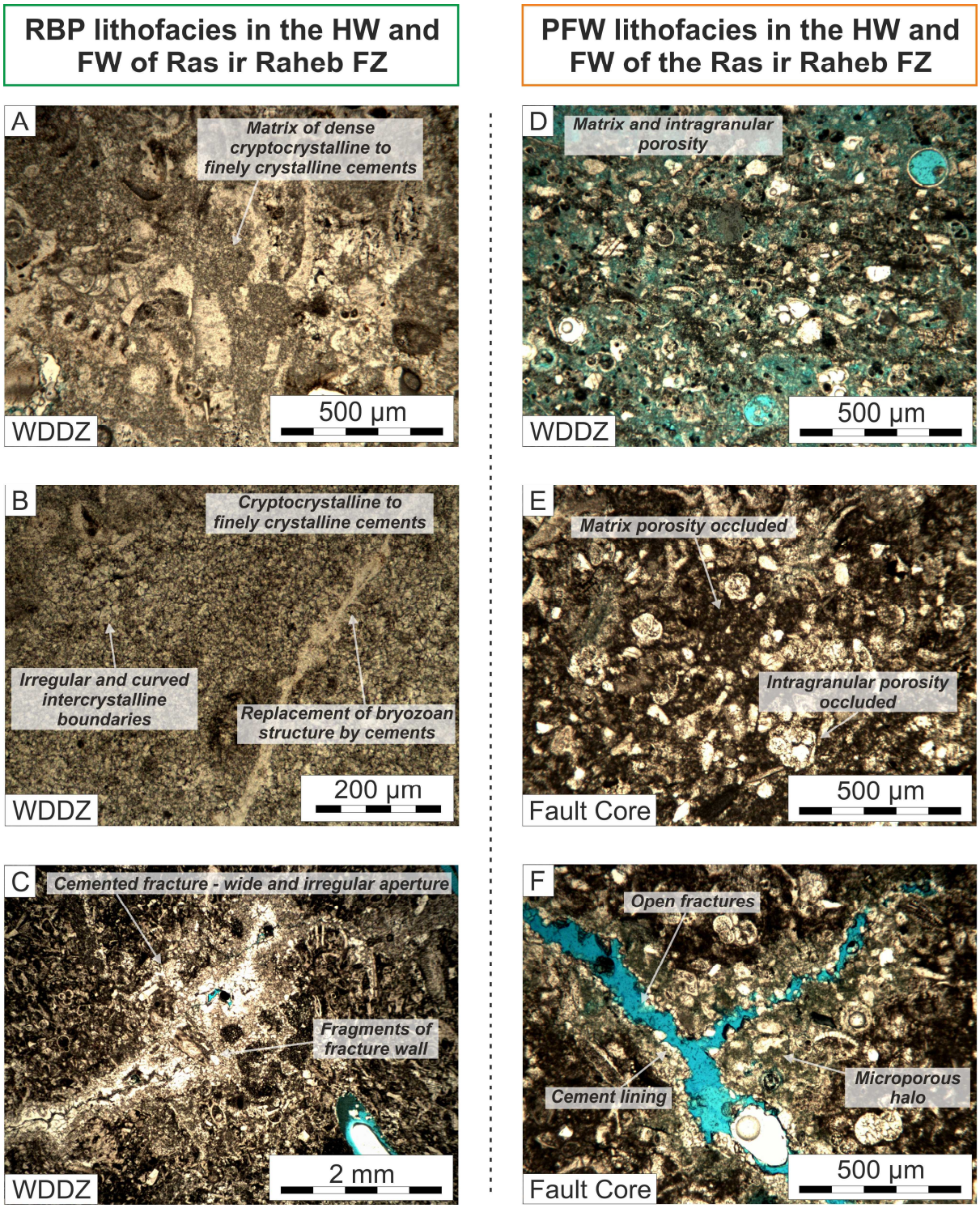

Figure 7 - Optical photomicrographs (PPL) displaying the key fault related diagenetic processes in the RBP and PFW lithofacies across the Ras ir Raheb Fault Zone. The photomicrographs are

annotated with the fault architectural element in which they are recorded. RBP lithofacies: A) and B) neomorphic calcite cement and C) neomorphic cement cross cut by fractures that are occluded by calcite cement. PFW lithofacies: D) no discernible fault related damage or diagenesis, E) microcrystalline calcite cementation of the matrix and F) fractures crosscutting the cemented matrix.

Two generations of fractures cross-cut, and hence postdate, the neomorphic cements in the fracture splay zone and the WDDZ. Both fracture generations have wide, irregular apertures and are associated with vugs (Figure 7 c). Calcite cementation has occluded the earlier generation of fractures (Figure 7 c), whereas the later generation remains open. In the fault core, brecciation postdates the neomorphic cementation (Figure 5). The matrix created by the brecciation is pervasively occluded by cryptocrystalline calcite cements.

In the PFW lithofacies, no fault related diagenesis is observed within the fracture splay zone or the WDDZ at distances of greater than 0.3 m (and -0.3m; negative distances equate to HW samples) from the PSS (Figure 7 d). In lenses on the PSS (i.e. -0.05 m into the HW), the matrix and primary pore volume are occluded by cryptocrystalline calcite cements (Figure 7 e). The occluded matrix is cross cut by fractures, which have a blue-green microporous halo that is indicative of minor dissolution (Figure 7 f). The fracture walls are lined by minor calcite cements (Figure 7 f).

4.2.4 Pore Systems

The spatial variation of pore sizes and pore types across the Ras ir Raheb Fault Zone in the studied lithofacies is displayed in figure 8. Generally, the pore volume composed of macro and meso pores decreases from the protoliths into the fault zone (Figure 8 a and b). In the RBP lithofacies, this pore volume decreases in two steps into the fault zone; at distances of approximately 12 m from the PSS (i.e. within the WDDZ) and in the fault core (Figure 8 a). Conversely, in the PFW lithofacies the decrease in the macro and meso pore volume is

restricted to the fault core only; in the damage zone in the HW and FW, the macro and meso pore volumes are approximately comparable to the protolith in this lithofacies (Figure 8 b).

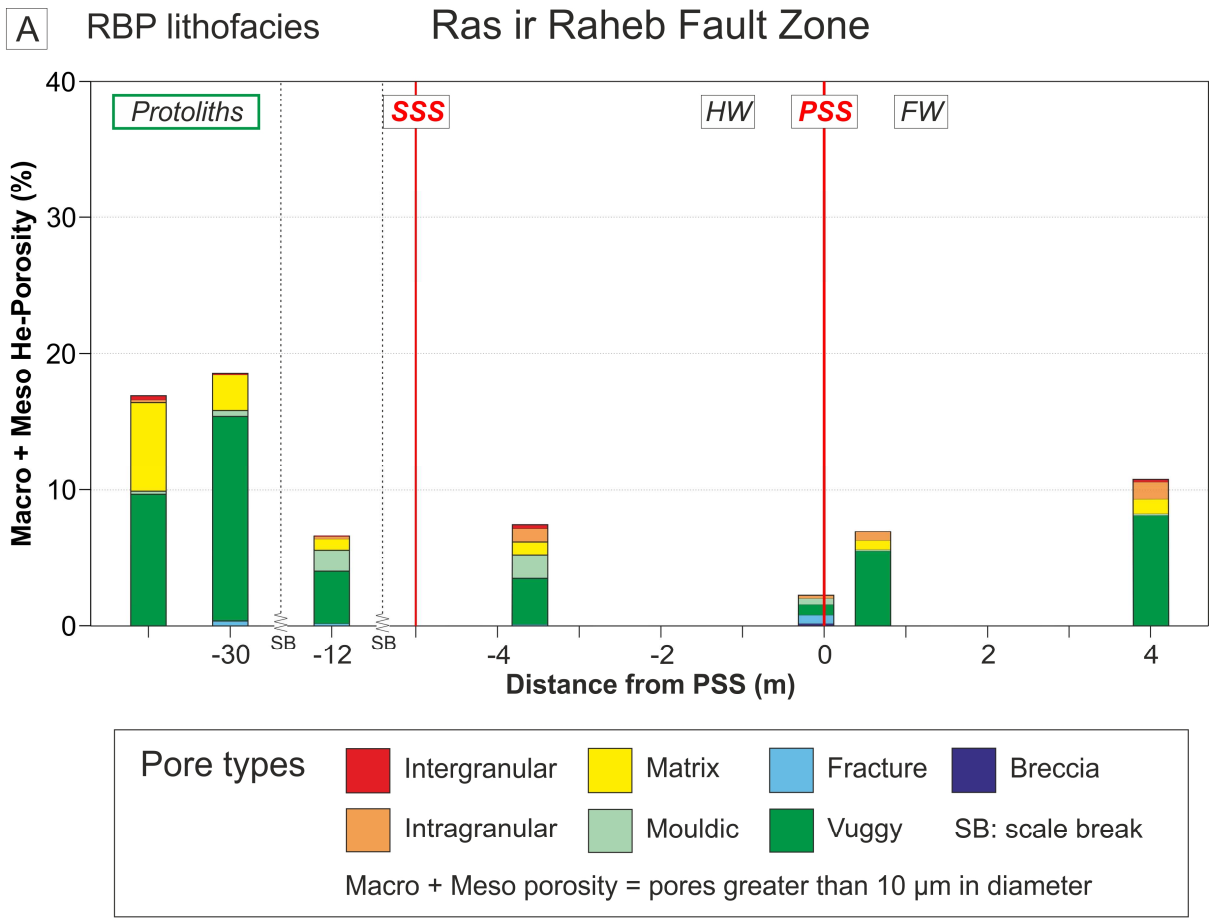

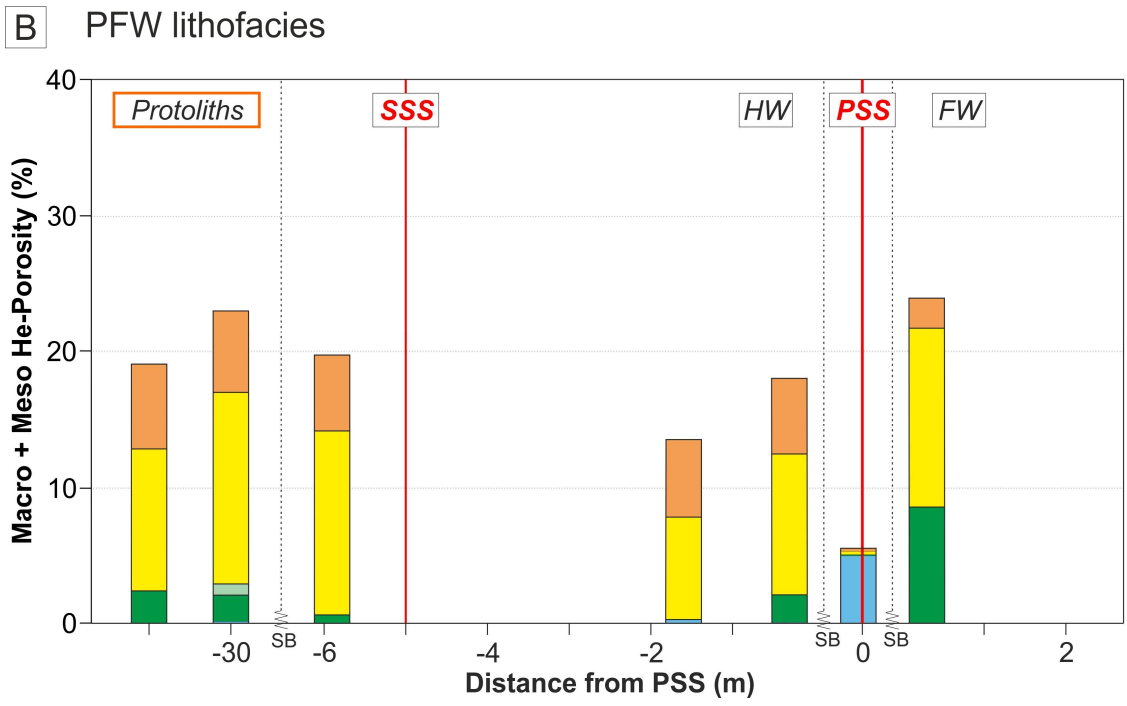

Fig 8 - Graphs displaying the variation in macro and meso pore volume (i.e. pores greater than 10µm in diameter) and pore types in the A) RBP lithofacies and B) PFW lithofacies across the Ras ir Raheb Fault Zone. Negative distances from the PSS correspond to HW samples, whereas positive distances represent FW samples. The pore volume composed of macro and meso pores is quantified using image analysis (see 3.5.1 Image Analysis), while the quantity of the different pore types are estimated using point count analyses (see 3.5.2 Point Count Analysis).

In the RBP lithofacies, the protoliths are dominantly composed of vuggy and matrix pore types. The pore volume composed of vuggy and matrix pore types decreases into the fault zone, while small quantities of mouldic and fracture pore types are formed (Figure 8 a). Generally, there is no significant change in the pore type composition in the PFW lithofacies across the Ras ir Raheb Fault Zone, except in fault core, where the primary pore types are significantly reduced and fracture pore types are created (Figure 8 b).

4.3 Victoria Lines Fault Zone

4.3.1 Fault Architecture

Similar to the Ras ir Raheb Fault Zone, three architectural elements are observed in the Victoria Lines Fault Zone (fault core, fracture splay zone and WDDZ). The fault core in this fault zone comprises breccias and cataclasites. Cataclasite is observed within a discontinuous lens, up to 0.5 m in thickness that is located adjacent to the PSS in the FW only (Figure 9 b). The cataclasites are composed of cataclased grains of the CAP/G lithofacies (Figure 10 a). Breccia lenses that are 3 m in thickness and are dominantly composed of the PFW lithofacies are observed adjacent to the PSS in the HW (Figure 9 b). These breccias can contain mm-scale, rounded clasts of the PFW lithofacies hosted within a matrix comprising cataclased CAP/G grains (Figure 10 b). A discontinuous lens of breccia is also observed in the FW adjacent the cataclasite (up to 1m from the PSS); this breccia is characterised by cm-scale CAP/G clasts, which comprise 85 % of the fault rock and hence define a crackle breccia type

(Figure 10 c; *cf*. Woodcock and Mort, 2008). In the HW, discontinuous breccia lenses originating from the PFW lithofacies are observed adjacent to subsidiary slip surfaces, most abundantly at distances of less than 5 m from the PSS; these breccias are also composed of cm-scale clasts and correspond to crackle, mosaic and chaotic breccia types (Figure 10 d; *cf*. Woodcock and Mort, 2008).

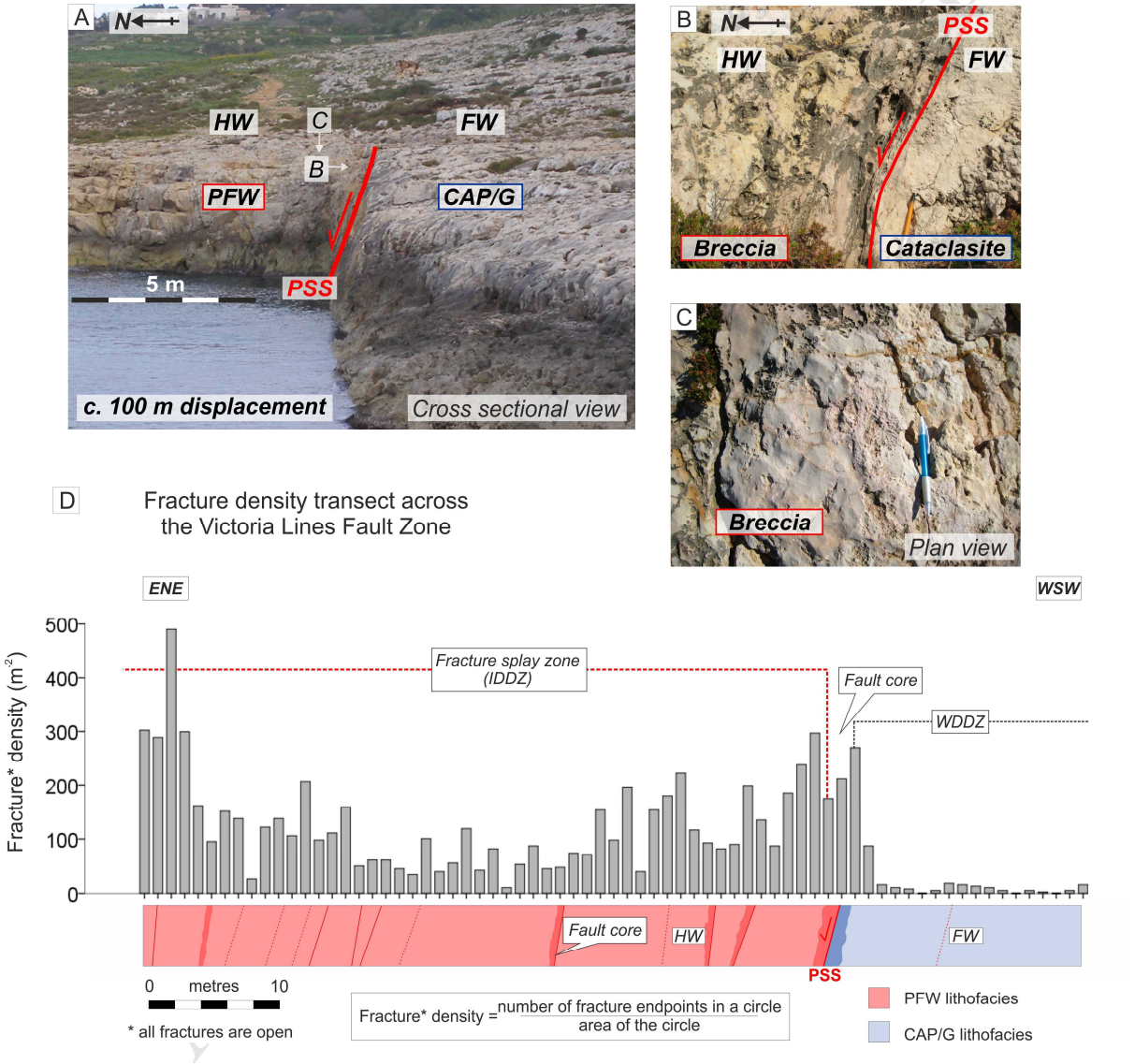

Figure 9 - An overview of the fault architecture in the Victoria Lines Fault Zone. A) Field photograph of the fault zone, highlighting the slip surfaces and the studied lithofacies. B) Field photograph of the fault rocks surrounding the PSS; a breccia lens in the PFW lithofacies (in the HW) and a cataclasite lens in the CAP/G (in the FW). C) Field photograph of a breccia lens in the

PFW lithofacies (in the HW). D) A fracture density transect across the Victoria Lines Fault Zone displaying the fault architecture. The positions of the fault rocks are displayed in A.

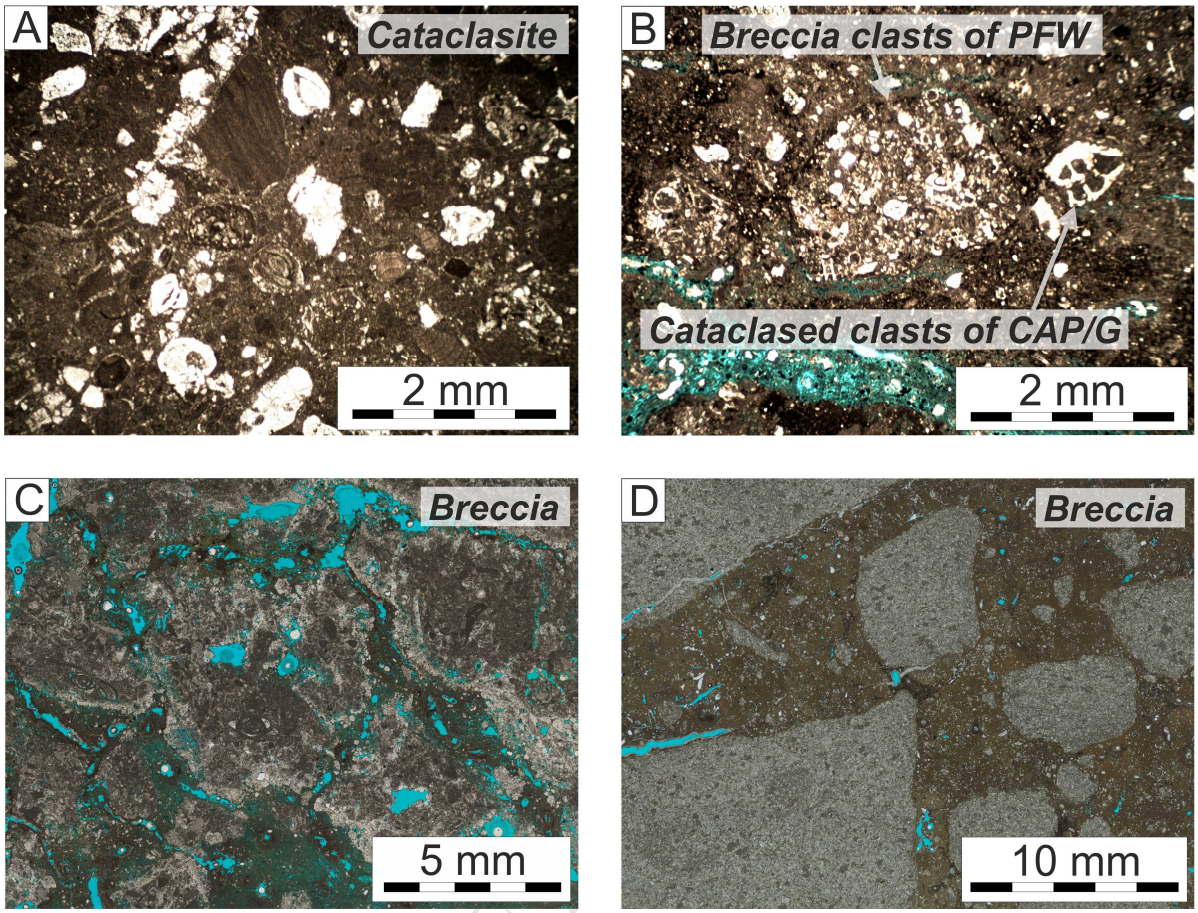

Figure 10 - Optical photomicrographs (PPL) of fault rocks in the Victoria Lines Fault Zone: A) Cataclasite in the FW adjacent to the PSS (CAP/G lithofacies; see Figure 9 b), B) breccia in the HW adjacent to the PSS (PFW lithofacies; see Figure 9 b), C) crackle breccia in the FW (CAP/G lithofacies) and D) chaotic breccia in the HW (PFW lithofacies).

Open fractures are observed within both lithofacies across the fault zone (Figure 9 d). Fracture densities are higher in the PFW lithofacies in the HW of the fault zone compared to the CAP/G lithofacies in the FW (Figure 9 d). For example, fracture densities of 100 m^{-2} are recorded in the CAP/G lithofacies adjacent to the PSS, whereas in the PFW lithofacies fractures densities of 300 m^{-2} are observed adjacent to the PSS (Figure 9 d). The higher fracture densities in the PFW lithofacies correspond to fracture splay zone, which is only

developed in the HW (i.e. only in the PFW lithofacies). The fracture splay zone extends in excess of 50 m into the HW, although the precise width of this damage zone remains unquantified due to the limited field exposure (Michie et al., 2014). It is expected that a major slip surface bounds the fracture splay zone and defines the transition into the WDDZ (Michie et al., 2014).

In the FW, the relatively low fracture densities in the CAP/G lithofacies correspond to the WDDZ (Figure 9 d). In this architectural element, fracture densities rapidly decreases away from the PSS, although fractures are recorded at distances of greater than 12.8 m from the PSS (Figure 9 d). Like the fracture splay zone in the HW, the width of the WDDZ is unknown due to the limited fault zone exposure.

4.3.2 Porosity and Permeability

Figure 11 displays the porosity and permeability in Victoria Lines Fault Zone organized according to lithofacies and fault architectural elements. In the CAP/G protolith, the porosity varies between 10 and 35 %, while the permeability is typically between 10 and 100 mD (Figure 11 a; blue shading). In the WDDZ, the porosity and permeability are either comparable or slightly reduced compared to the protolith, although permeability can be greater than 1000mD (1240mD; Figure 11 a). In the fault core originating from the CAP/G lithofacies, porosity is between 2 and 12 %, although, typically it is less than 5 %, while permeability ranges from 0.0001 to 44mD (Figure 11 a).

Due to sampling constraints, the protoliths of the PFW lithofacies were not sampled, however, based on core plugs that display no fault damage or fault related diagenesis, the protolith porosity and permeability are assumed to be c. 30 % and c. 10 mD respectively (Figure 11 b, red shading). In the corresponding lithofacies in the fracture splay zone and fault core, porosity and permeability are variably reduced compared to the protolith; the

porosity varies between 1 and 25 % whereas the permeability ranges from 0.0001 and 10 mD (Figure 11 b).

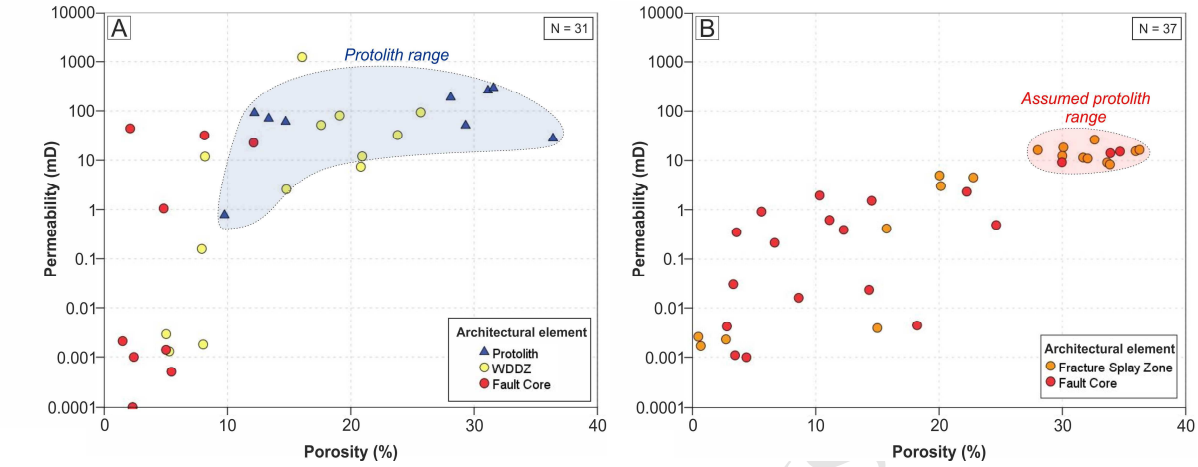

Figure 11- Cross plots of porosity-permeability subdivided according to the protolith lithofacies and the fault architectural elements in the Victoria Lines Fault Zone: A) CAP/G lithofacies and B) PFW lithofacies.

4.3.3 Fault Related Diagenesis

In the CAP/G lithofacies, the micritic matrix and bioclasts are replaced by cryptocrystalline to medium crystalline calcite cements (Figure 12 a and b). These cements are considered to be neomorphic in origin based on the following characteristics (Bathurst, 1975; Tucker et al., 1990): 1) the irregular crystal size distributions (Figure 12 b), 2) the presence of embayed and irregular shaped bioclastic debris floating within the calcite cements (Figure 12 b) and 3) the relict grains that are replaced with increasing calcite crystal sizes (Figure 12 a). The neomorphic cements are observed throughout the WDDZ however, they increase in abundance towards the PSS; they are patchily distributed at distances of 12.8 m (from the PSS), whereas at distances of 7.9 m or less, the neomorphic cements are pervasive (Figure 12 a and b). The neomorphically cemented matrix is crosscut by vugs (Figure 12 c and d), which are observed throughout the WDDZ (see Figure 14). The vuggy porosity is commonly associated with dissolution enhanced fractures, particularly at distances of less than 2.2 m

from the PSS. Vuggy and dissolution enhanced fracture pores are lined with finely to coarsely crystalline, calcite cements (Figure 12 c and d); these cements line vugs at distances of up to 7.9 m from the PSS (in the WDDZ), however, they are most abundant in a zone that extends from the PSS to 2.2 m into the FW. In the fault core, at distances of 0.3 m from the PSS, fault breccia clasts, which are composed of neomorphic cement, are fringed by calcite cements and crosscut by vugs that are lined by calcite cements (Figure 12 d). In the fault core adjacent to the PSS, fractures that are enhanced by dissolution, cross cut the cataclasite (Figure 10 a) and neomorphically cemented matrices.

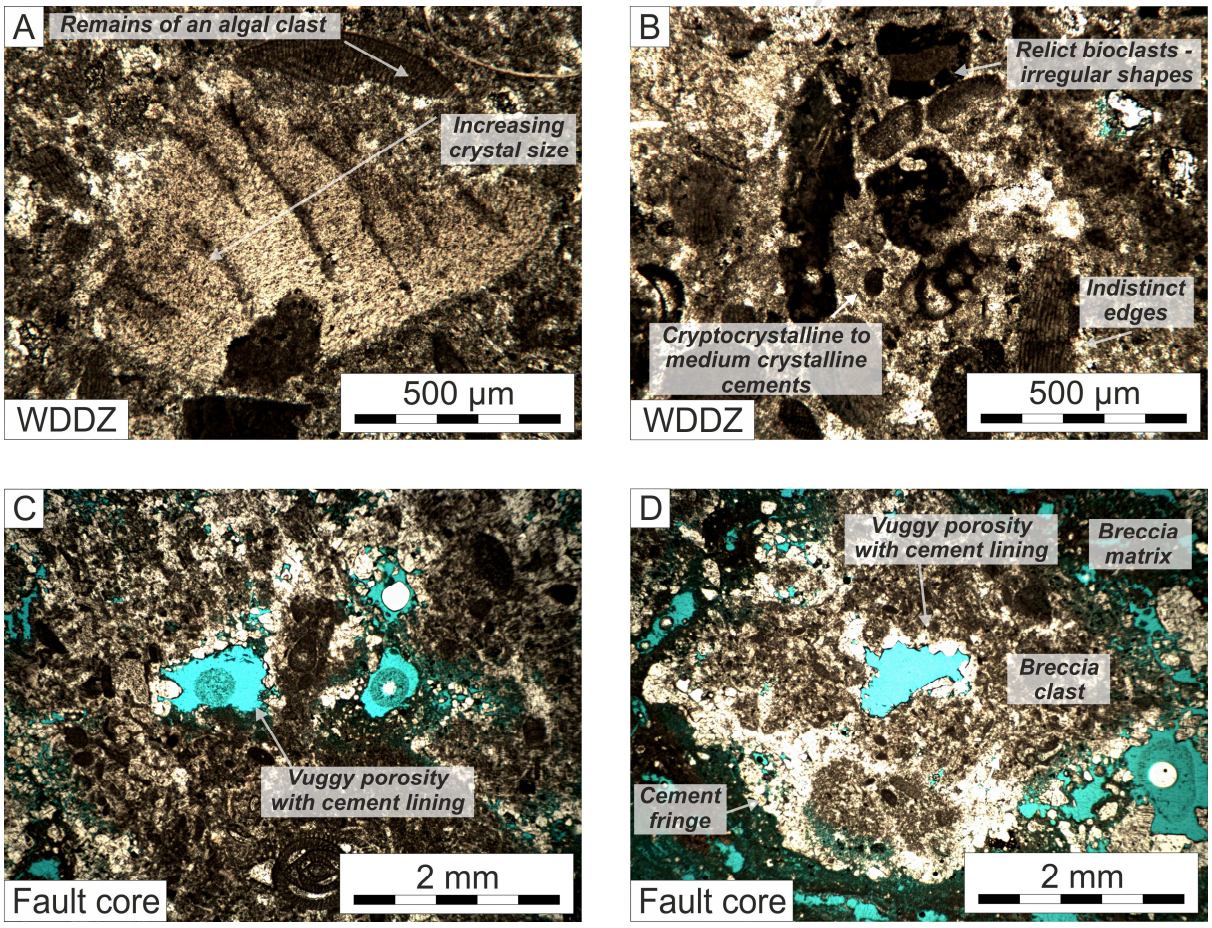

Figure 12 - Optical photomicrographs (PPL) displaying the key fault related diagenetic processes in the CAP/G lithofacies in the FW of the Victoria Lines Fault Zone. A) and B) matrix and allochems are replaced by neomorphic cement. C) dissolution has created vuggy pores in the neomorphically

cemented matrix; the vugs are lined with calcite cements. D) breccia clasts composed of neomorphic cements are crosscut by vugs and are fringed by calcite cements.

In the fracture splay zone at distances of greater than -5 m from the PSS, fault related diagenesis in the PFW lithofacies is limited to dissolution, which is focussed along fractures. At distances of -5 m or less from the PSS, pedogenic fabrics, including root moulds, alveolar septa textures, peloidal textures, *Microcodium*, root petrifications and laminar cryptocrystalline cements are commonly hosted within or surrounding fractures or fault brecciated matrices (Figure 13 a). The pedogenic fabrics are considered to have formed after the onset faulting due to their occurrence within and surrounding these fault related structures only. Fault breccia clasts are replaced by cryptocrystalline calcite cements at distances of less than -5 m in the fracture splay zone, (Figure 13 b, c and d). The cryptocrystalline calcite replacement is typically pervasive at the edge of fault breccia clasts but decreases into their centre; this trend is shown by an increase in the preservation of planktonic foraminifera from the edge (Figure 13 c) to the centre of clasts (Figure 13 d). This replacement cementation is thought to be related to the pedogenesis (Arakel, 1982).

In the fault core adjacent to the PSS (see Figure 9 b), rare syntaxial calcite veins, which are approximately 4 to 5 mm in width, are observed (Figure 13 e). The calcite veins contain wall rock inclusions, which are indicative of a crack-seal evolution (Bons et al., 2012). In areas adjacent to the calcite veins, relict pedogenic textures, such as root casts, and irregular shaped peloids are observed floating within a cement matrix, which is composed of radial, fibrous and inequigranular, xenotopic calcite (Figure 13 f). The habits and coarse crystal sizes of these replacive cements are characteristic of neomorphic calcite (Bathurst, 1975). Fractures that are enhanced by dissolution, cross cut the neomorphically replaced matrices.

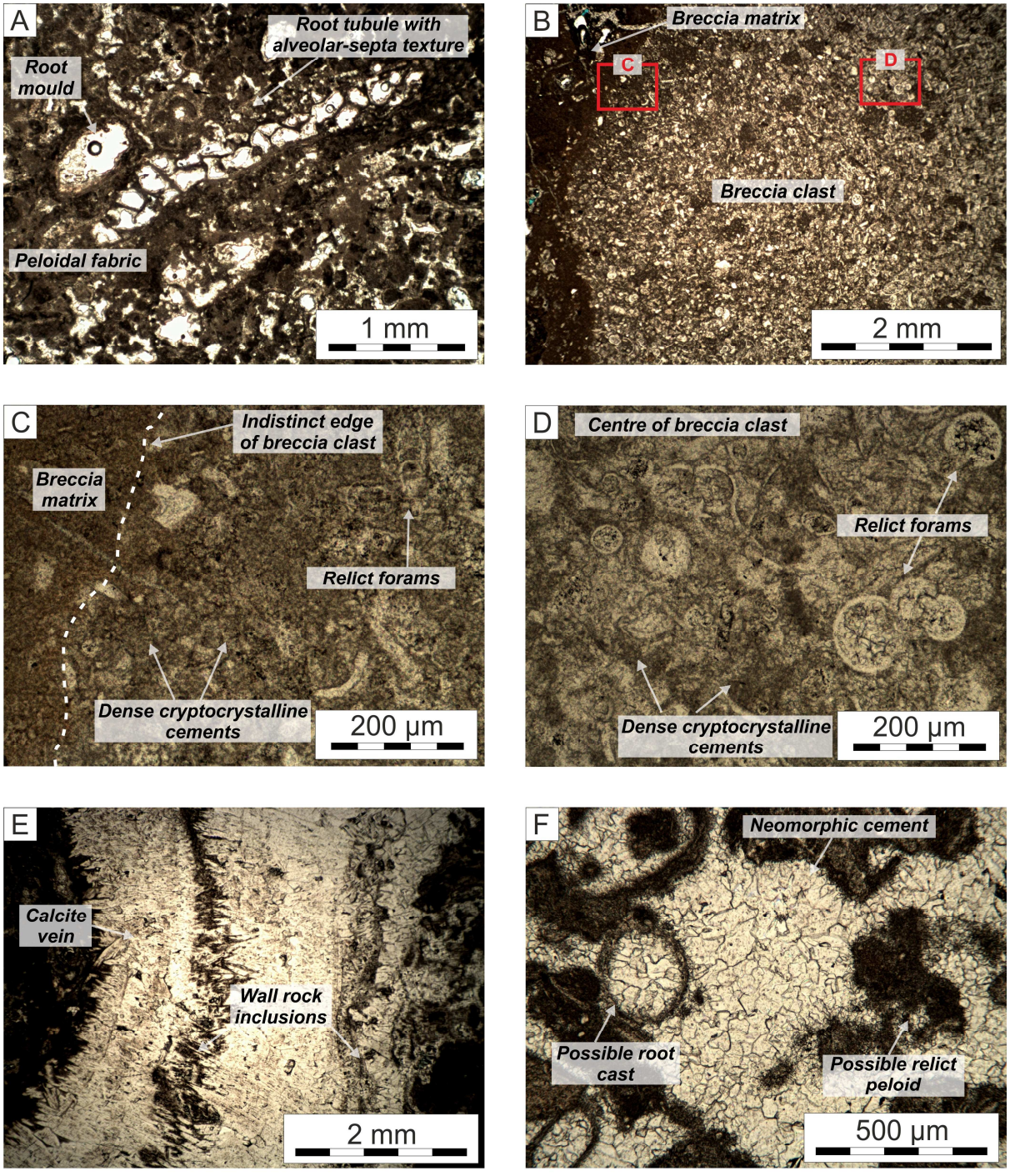

*All photomicrographs are taken from the fault core

Figure 13 - Optical photomicrographs (PPL) displaying the key fault related diagenetic processes in the PFW lithofacies in the HW of the Victoria Lines Fault Zone. A) pedogenic features, such as root moulds and tubules, in a breccia matrix. B) a breccia clast replaced by cryptocrystalline cement. C) the edge of the breccia clast shown in B with poorly preserved planktonic foraminifera in a cryptocrystalline matrix. D) the centre of the breccia clast shown in B with well-preserved

planktonic foraminifera in a cryptocrystalline matrix. E) calcite vein with wall rock inclusions. F) inequigranular, xenotopic neomorphic cements replacing a possible root cast and peloids.

4.3.4 Pore Systems

Figure 14 displays the spatial variation in pore sizes and pore types across the Victoria Lines Fault Zone. The pore volume composed of macro and meso pores generally decreases from the protoliths through the damage zones and into the fault core in both lithofacies (Figure 14).

In the CAP/G lithofacies (in the FW), the total pore volume composed of macro and meso pore sizes decreases from 21-28 % in the protoliths to a minimum of 11 % in the WDDZ and to c. 2 % in the fault core (Figure 14). Similarly, in the PFW lithofacies (in the HW), 25 % total porosity is composed of macro and meso pore sizes in the assumed protoliths, while in the same lithofacies in the fault core, macro and meso pore sizes only comprise 3-5 % total pore volume (Figure 14). This decrease is localised to distances of 2 m or less from the PSS in the PFW lithofacies (i.e. fracture splay zone and fault core), while in the CAP/G lithofacies, a gradual decrease is observed throughout the WDDZ (Figure 14).

There is a transition from pore systems dominated by primary pore types in the PFW and CAP/G protoliths to pore systems dominated by secondary pore types into the fault zone (Figure 14). In the CAP/G lithofacies, intergranular and matrix pore types are occluded , while vuggy, fracture and mouldic pore types are created in the WDDZ at distances of 12 m or greater from the PSS (Figure 14). A similar transition from primary pore types (dominantly matrix and intragranular pores) to secondary pore types (mouldic, vuggy and fracture pores) is observed within the fracture splay zone and fault core in the PFW lithofacies, however this change is localised to within 4 m of the PSS in this lithofacies.

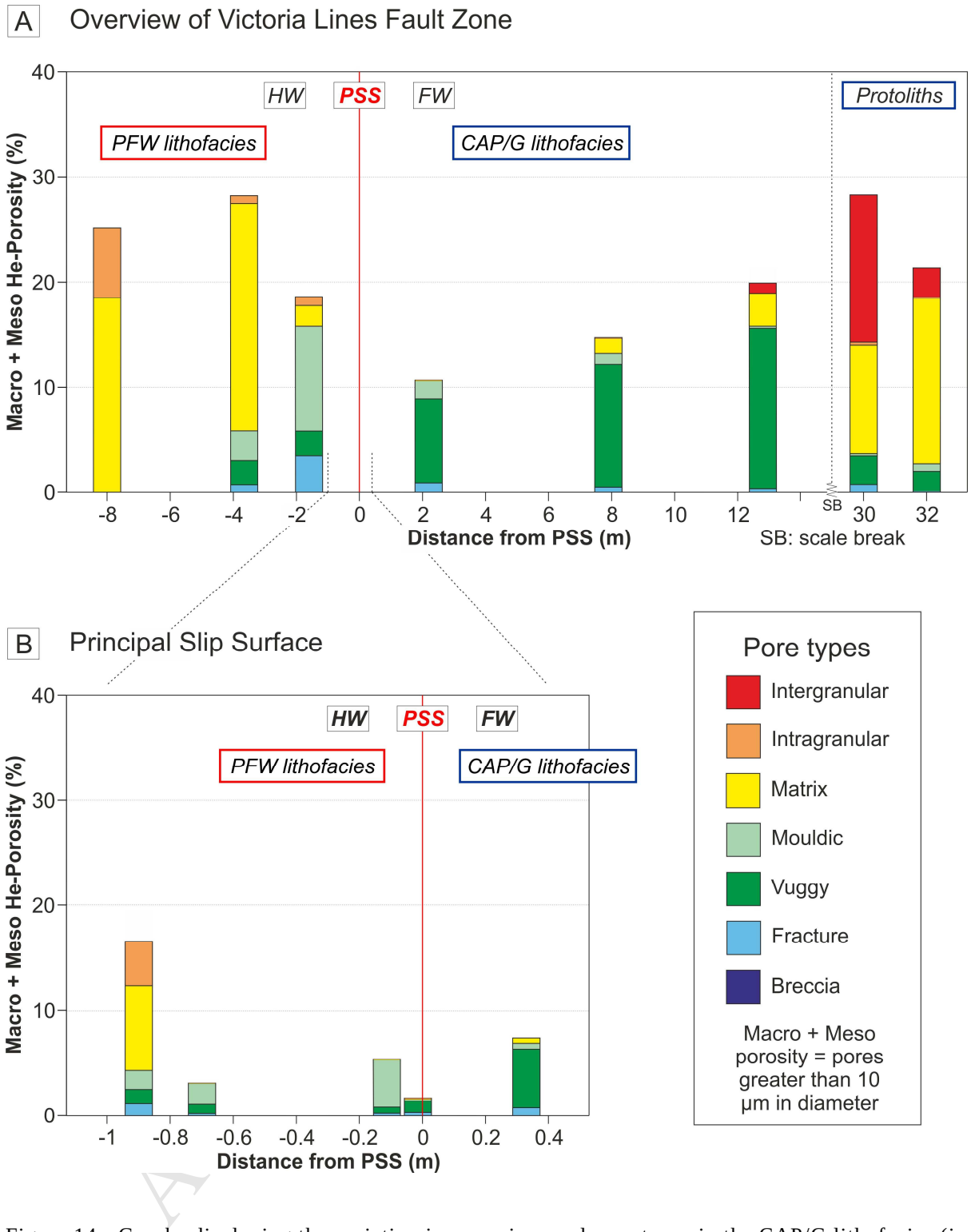

Figure 14 - Graphs displaying the variation in pore sizes and pore types in the CAP/G lithofacies (in the FW) and PFW lithofacies (in the HW) across the Victoria Lines Fault Zone. A) Overview of the fault zone and B) the principal slip surface (PSS). Negative distances from the PSS correspond to HW samples, whereas positive distances represent FW samples.

5 Discussion

5.1 Textural Evolution

A range of diagenetic and deformation processes are observed within the Ras ir Raheb and Victoria Lines fault zones. In order to understand the evolution of permeability across the fault zones, it is first necessary to understand the processes that modify the textures and the controls on these modifications.

In both the studied fault zones, neomorphic cements are observed within the packstone (Figures 7 a, b and c) and pack-grainstone lithofacies (Figure 12 a and b) within the damage zones. Timing relationships suggest that this is the first fault related process that has affected these lithofacies. Neomorphic cements are result from the process of aggrading neomorphism, which is the transformation of micrite to microspar (Bathurst, 1975). This process is common in the rock record (Caron and Nelson, 2009; Dorobek, 1987; Maliva and Dickson, 1992); its occurrence within the carbonate sediments of the Maltese Islands would be unsurprisingly and yet, it is largely absent from these sediments, except within and surrounding fault zones in the grain-dominated lithofacies. Aggrading neomorphism is likely to have resulted from early fault stresses in the presence of diagenetic fluids, which considering the shallow burial of the sediments on the Maltese Islands (Bonson et al., 2007) could originate from marine, meteoric or shallow burial fluids. This process has not been previously recorded as a fault related process to the author's knowledge, however a variety of similar processes are documented. Matonti et al. (2012) document calcite cements in grain supported carbonate lithofacies surrounding the Castellas Fault Zone in the southeast of France. In the Castellas Fault Zone, the cements are pore filling and originate from $CaCO_3$-rich fluids derived from fault related pressure solution. Similar pressure solution driven cementation processes are observed in micritic carbonates and chalks around fault zones

(Carrio-Schaffhauser and Gaviglio, 1990; Gaviglio et al., 1999). This type of cementation is distinguishable from aggrading neomorphism as it is pore filling rather than replacive. Dynamic recrystallisation is an intracrystalline plastic deformation mechanism that is commonly recorded in fault rocks (Knipe, 1989; Sibson, 1977); it is typically identified by a reduction in crystal sizes compared to the undamaged equivalent lithology (Etheridge and Wilkie, 1979; Sibson, 1977). In the fault zones in this study, crystal sizes increase (e.g. Figure 8 a), therefore this process is not thought to be dynamic recrystallisation.

In contrast, in the wackestone lithofacies in the studied fault zones, the first fault related process is fracturing; fracturing does, however, occur within packstone and pack-grainstone lithofacies following aggrading neomorphism (Figure 7 c). Fracturing is a common fault damage process within limestones and chalks (Corbett et al., 1987; Lavenu et al., 2014; Petracchini et al., 2012).

There is no evidence in this study to suggest that the aggrading neomorphism in the packstones and pack-grainstones and fracturing in the wackestones are coeval. On the contrary, the aggrading neomorphism could be an initial response to low stresses within the packstones and pack-grainstones, while the fracturing, in both the packstones/ pack-grainstones (following aggrading neomorphism) and wackestones could relate to subsequent higher stresses. These timing relationships remain unclear in this study.

Fault breccias are observed within discontinuous lenses on or surrounding the PSS in both fault zones and in both lithofacies. Brecciation resulting from faulting is commonly reported in carbonate lithologies (Agosta et al., 2012, 2010; Bastesen and Braathen, 2010; Storti et al., 2003; Tarasewicz et al., 2005). The breccias in this study are created by hydraulic brecciation of the existing fractures as a result of increasing shear stress and pore pressures (Michie, 2015).

Fracturing and brecciation enhance the diagenetic potential of a rock by providing pathways for diagenetic fluids. Following fracturing and brecciation, the textural evolution in the wackestones and the packstones and pack-grainstones reflects the enhanced diagenetic potential of the rock. The diagenetic processes that occur therefore depend on the diagenetic fluids and the diagenetic environment in which the rock is positioned. Bonson et al. (2007) suggest that the carbonate succession on the Maltese Islands has only been buried to 300 m or less, which, restricts diagenesis to shallow burial and meteoric environments (Knoerich and Mutti, 2006). Three processes, representing diagenesis within such environments, are observed within the studied fault zones. Fracture and breccia porosity are enhanced (Figures 10 c and 12 c and d), while vugs are created, particularly adjacent to the fractures and within the breccia matrices and clasts, indicating that dissolution is occurring. This secondary porosity is lined by minor, coarsely crystalline equant calcite cements (Figure 12 c and d). Pedogenic textures, including root moulds (Figure 13 a), observed within and surrounding fractures and breccia matrices only, suggest that pedogenesis has also occurred due to the enhanced diagenetic potential of these rocks specifically within in a vadose meteoric environment. Pedogenesis includes the replacement of primary textures by cryptocrystalline calcite cements (Arakel, 1982) particularly at the edges of breccia clasts and on walls of fractures (Figure 13 c).

Fractures cross-cut other fractures which display diagenetic alteration, as well as brecciated textures and/or pedogenically altered textures. This suggests that fracturing and brecciation are either episodic and punctuated by diagenetic modifications or prolonged with coeval diagenetic alterations.

A *c.* 50 cm thick zone of cataclasite is observed on the PSS in the pack-grainstone lithofacies in the Victoria Lines Fault Zone; cataclasite is not observed within the wackestone lithofacies in this fault zone nor is it observed within the packstones and wackestones in the Ras ir

Raheb Fault Zone. This cataclasite is created by attritional brecciation, which includes grain-scale fracturing and crushing, grain sliding and rotation and pore collapse (Engelder, 1974; Micarelli et al., 2006; Sibson, 1986). The diagenetic potential of cataclasite is relatively low as a result of pore collapse and the resultant low porosity and permeability. Consequently, diagenetic modifications do not follow cataclasis.

5.1.1 Controls on the Evolution of Textures

The types of deformation and diagenetic alteration that occur in the studied fault zones depend upon the primary lithofacies and to a lesser extent the fault displacement; this section details the likely controls on the processes that are observed within these fault zones. Such controls can be used as a predictive tool to understand how textures are modified by faulting.

Aggrading neomorphism occurs in the packstone and pack-grainstone lithofacies in both fault zones. Bausch (1968) shows that recrystallisation of micrite to microspar is inhibited when the clay content within the micrite matrix is in excess of 2 %. SEM imaging and associated energy-dispersive X-ray spectroscopy (EDS) within the wackestones suggests that the clay content is greater than 2 %. As a result of this clay, aggrading neomorphism is likely to be inhibited within the wackestone lithofacies (Bausch, 1968). On the contrary, no clay is observed within the packstones and pack-grainstones. The allochem assemblage within these lithofacies is dominantly characterised by coralline algae, bryozoa and benthic foraminifera. Coralline algae are composed of high-Mg calcite (Hood and Nelson, 1996; Scholle and Ulmer-Scholle, 2003), which is metastable and hence susceptible to replacement. Furthermore, the wackestones are dominantly composed of planktonic foraminifera, which due to their low-Mg calcite composition (Hood and Nelson, 1996), are comparatively stable and thus not susceptible to replacement. It therefore is likely that the mineralogical composition of these lithofacies promotes or inhibits aggrading neomorphism.

Fracturing is common in low porosity and/ or densely cemented lithofacies (Fossen et al., 2007; Underhill and Woodcock, 1987; Vajdova, 2004). The packstone and pack-grainstones are typically low to non-porous and densely cemented following aggrading neomorphism; these textural changes are likely to have promoted fracturing. Similar textural transformations, and associated changes in the mechanical properties, correspond to the formation of fractures and faults within grainstones (Tondi, 2007).

The average porosity of the wackestones, prior to faulting, is assumed to be c. 30 % based on the undamaged lithofacies. Additionally, these lithofacies are only weakly cemented (Figure 2 b and d). Rath et al. (2011) shows that weakly cemented, high porosity grainstones deform by cataclasis, although pressure solution at grain contacts, and related cementation, is also observed in grainstones (Tondi, 2007) as well as micritic limestones (Carrio-Schaffhauser and Gaviglio, 1990). The textural characteristics of the wackestones therefore may suggest that they are likely deform by cataclasis or pressure solution (Carrio-Schaffhauser and Gaviglio, 1990; Fossen et al., 2007; Underhill and Woodcock, 1987) and yet they fracture. The formation of through-going fractures in porous rocks requires a low contrast in physical properties between the matrix and the grains as well as a degree of cementation (Groshong, 1988). The homogeneous texture and the corresponding absence of significant mechanical heterogeneity, coupled with small amounts of cement are likely to promote fracturing in the wackestones.

As previously mentioned, breccias evolve from the existing fractures by means of hydraulic brecciation due to increasing shear stresses and pore pressures (Michie, 2015). The development of fractures within both lithofacies in the studied fault zones therefore promotes brecciation. However, as a result of greater shear stress, the thickness of the breccia lenses is greater in the higher displacement fault zones; similar thickness-displacement trends are

commonly reported to follow power law relationships (Bastesen and Braathen, 2010; Evans, 1990; Shipton et al., 2006).

In the fault core of the Victoria Lines Fault, cataclasis has occurred in the pack-grainstones only. This deformation mechanism is prevalent in this lithofacies as a result of its high porosity and relatively weak cementation (Fossen et al., 2007; Underhill and Woodcock, 1987), which promote grain-scale deformation. Zhang et al. (1990) show that the grain size of sandstones can control the mechanism by which its deforms; a lower critical pressure is required to deform relatively coarse and porous sandstones by grain crushing compared to fine-grained and lower porosity sandstones. It is therefore possible that cataclasis does not occur in the wackestones in this fault zone as a result of their comparatively fine grain size.

5.2 Pore System Controls on Permeability

The documented textural changes impact the permeability by modifying the pore systems. This section of the study quantifies the impact of pore system characteristics, such as pore sizes and types, on permeability; this understanding is then integrated with the textural evolution and pore system trends to discuss the evolution of permeability across the fault zones.

Weger et al. (2009) document a general trend of high permeability for a given porosity corresponding to the largest pore sizes. Melim et al. (2001) similarly suggest that macro porosity has a stronger influence on permeability than total porosity and that the connectivity of macro pores is the single most important factor controlling permeability. In this study, the permeability has a good positive correlation ($R^2 = 0.76$) with combined macro and meso porosity (i.e. pore sizes greater than 10 µm in diameter) (Figure 15 a), indicating that pores greater 10 µm in diameter are dominantly contributing to the permeability, rather than smaller pores.

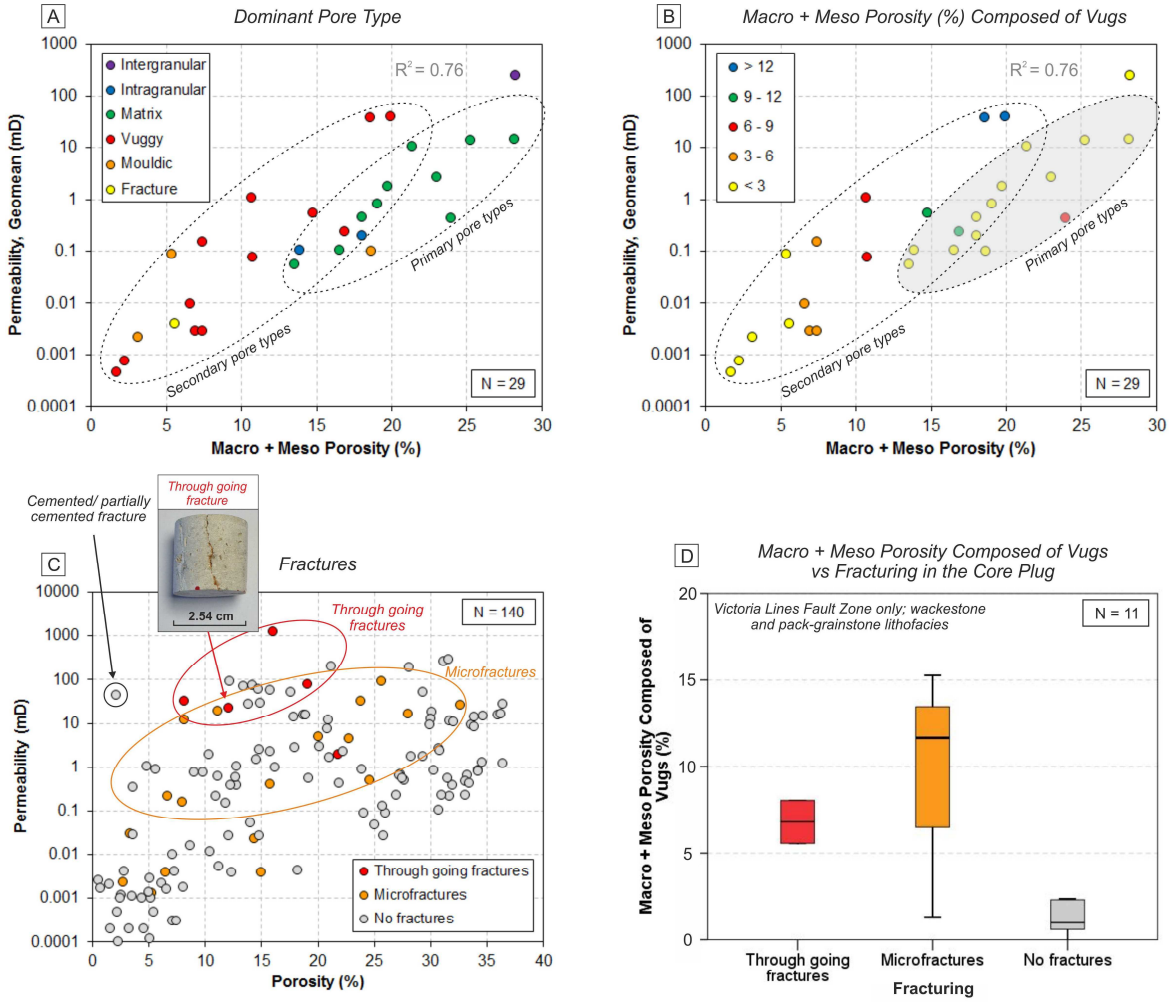

Figure 15 - Graphs displaying the pore system controls on permeability. Cross plots of macro and meso porosity and permeability (geomean) subdivided according to A) the dominant pore type and B) the amount of vuggy macro and meso porosity. C) Cross plot of porosity and permeability subdivided according to the degree of core plug fracturing. D) Box and whisker plot of the quantity of vuggy macro and meso porosity according to the degree of core plug fracturing.

Anselmetti et al. (1998) show that macro porosity is an important control on permeability, but also that, scatter in this relationship is introduced by non-connected isolated pore types such as mouldic pores. Figure 15 a shows that for a given quantity of macro and meso porosity, the permeability broadly varies according to the pore type. Primary pore types, such as intragranular and matrix pores, tend to have 1 to 2 orders of magnitude lower permeability at the same macro and meso porosity compared to secondary pore types, such as vugs and

moulds. However, below 10 to 15 % macro and meso porosity, this relationship between pore sizes and types and permeability becomes unclear due to the paucity of data.

Lucia (1983, 1995) divide vugs into touching and separate types; touching vugs can form interconnected pore systems that enhance permeability, while separate vugs tend to be isolated and hence associated with low permeabilities (Loucks, 2002; Lucia, 1995, 1983; Melim et al., 2001). Figure 15 b shows that the permeability associated with secondary pore systems is controlled by the amount of vuggy macro and meso pores; larger quantities of these pores correspond to relatively high permeabilities. This suggests that pore connectivity increases with greater amounts of vugs and that small quantities of vugs, e.g. < 6 %, are possibly isolated, i.e. separate vugs (Lucia, 1995, 1983), and hence correspond to low permeabilities (Figure 15 b).

Fractures are observed on the field and thin section-scale in the Ras ir Raheb and Victoria Lines fault zones (Figures 4 d, 7 c and f and 9 d); open and interconnected, fractures are commonly considered to increase permeability (Agosta et al., 2010; Larsen et al., 2010; Matonti et al., 2012; Nelson, 1985). To assess the impact of fracturing on permeability, core plugs have been qualitatively subdivided into three categories based on their degree of fracturation: 1) through going fractures, 2) microfractures and 3) no fractures. Through going fractures traverse the entire length of the core plug, while fractures that incompletely traverse a core plug are termed microfractures. In both instances, the fractures are open with a minor calcite cement lining (e.g. Figure 15 c); this cement lining is likely to prevent core plug failure, which is typical in fractured core plugs during permeability measurements. Figure 15 c shows that permeability, at a given total porosity, is typically higher in core plugs containing through going and to a lesser extent microfractures compared to those core plugs which contain no fractures. Therefore, in agreement with previous studies (Agosta et al.,

2010; Larsen et al., 2010; Matonti et al., 2012; Nelson, 1985), this study shows that open fractures increase permeability.

Figure 15 d shows that core plugs containing both through going and microfractures are associated with larger quantities of vuggy macro and meso pores compared to core plugs without fractures. This is consistent with thin section observations of vuggy pores concentrated around fractures (e.g. Figure 10 c). Furthermore, this indicates that fracturing enhances the diagenetic potential of these rocks, promoting processes such as dissolution. However, the amount of vuggy macro and meso porosity is not associated with the extent of fracturing at the core plug scale; larger quantities of vugs are observed in core plugs with microfractures compared to through going fractures. This may suggest that through going and microfractures observed in the core plugs are not completely representative of the fracture networks at the field scale; microfractures are possibly better connected at the field scale and hence have a higher diagenetic potential, leading to the creation of larger quantities of vuggy pores.

5.3 Permeability Evolution

The pore system controls on permeability are integrated with the pore system trends across the fault zones (Figures 8 and 14) to understand the temporal and spatial evolution of permeability according to faulting.

Two categories of deformation and diagenetic processes occur in the studied fault zones: 1) porosity occlusion processes, such as aggrading neomorphism and cataclasis, and 2) porosity creation processes, including fracturing, brecciation and dissolution. The processes that occur largely depend on the primary lithofacies (grain vs micrite supported), the fault zone displacement and the position within the fault zone (damage zone vs fault core) (Figures 16

and 17), however, they also reflect and the diagenetic environment in which the rocks are positioned.

5.3.1 Grain Supported Lithofacies

Aggrading neomorphism occludes the macro and meso porosity in the packstone and pack-grainstone lithofacies up to distances of c. 12 m from the PSS (into the HW and FW) in the damage zones in both the low and high displacement fault zone (Figures 8 and 14). This process, where pervasive, causes permeability to decrease (relative to the protolithology) to a minimum of 0.001mD (Figure 16).

The mechanical properties of the grain supported lithofacies are modified as result of the aggrading neomorphism. This modification leads to fracturing in the damage zones and brecciation in the fault core in both the low and high displacement fault zone (e.g. Figures 5, 7 c, 10 c and 12 d). Fracturing and brecciation enhance the permeability and hence the diagenetic potential of the rock promoting diagenesis. The diagenetic processes that follow depend upon the diagenetic environment in which the rock is situated. For example, meteoric processes dominated by dissolution are observed in the grain supported lithofacies in the studied fault zones. Dissolution creates vuggy macro and meso pores (e.g. Figures 12 c and d), which increases permeability to varying degrees depending on the extent of their development (Figure s 15 b and 16). It is likely that large quantities of vuggy macro and meso pores, associated with relatively high permeabilities, develop due to the presence of open and well-connected fracture networks. Due to the high fracture densities recorded in the fault zones (Figures 4 d and 9 d) and the comparatively low number of fractured core plugs (23 out of 140), a bias exists in the sample database. As a result, permeability values are assumed to be under-representing optimal flow paths in the fracture and vuggy pore systems (Ehrenberg, 2007; Vik et al., 2013) and are therefore expected be lower than the bulk rock permeabilities. However, the bulk rock permeabilities are not quantified in this study.

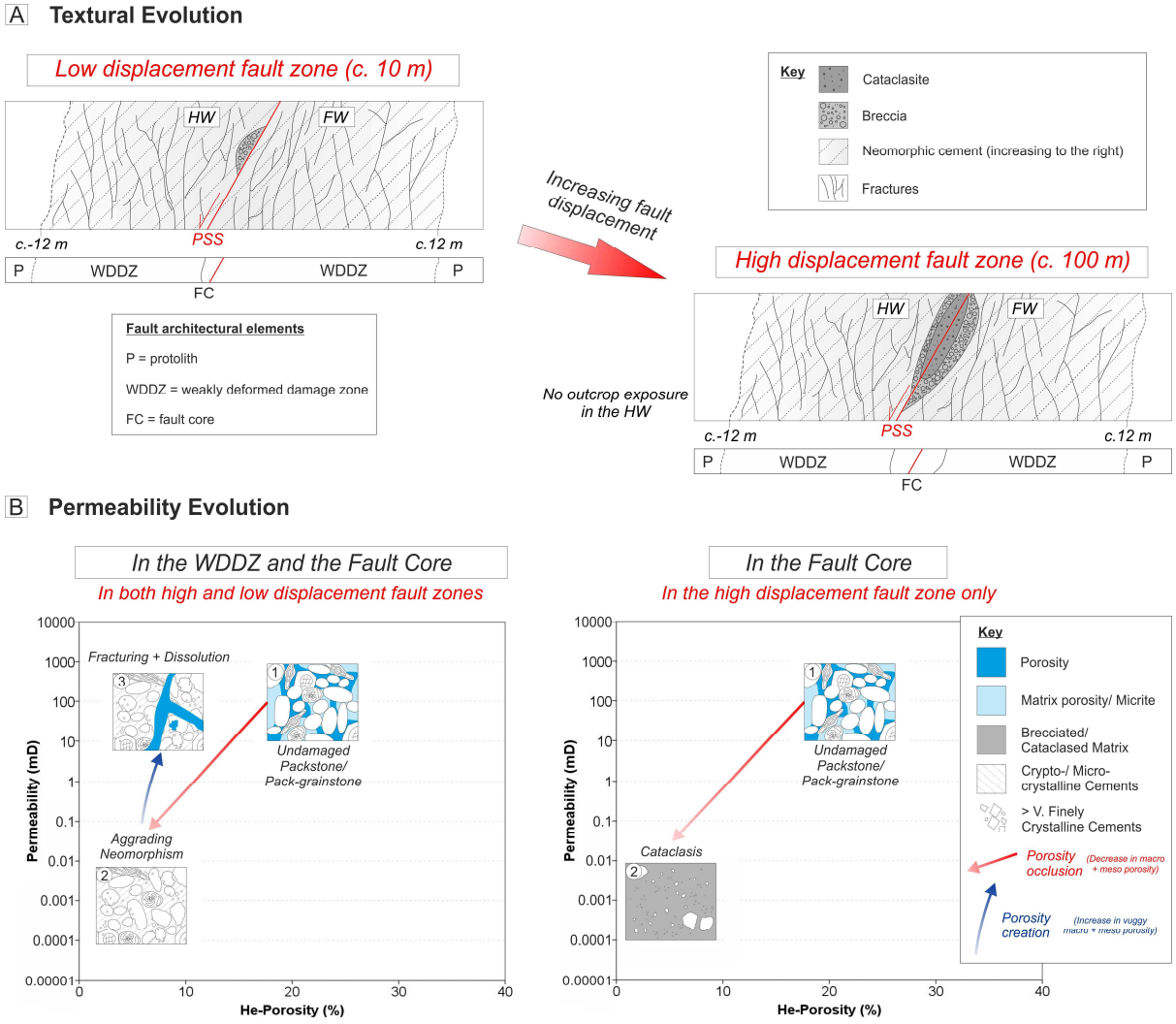

Figure 16 - Spatial and temporal evolution of A) textures and B) porosity and permeability in the packstone and pack-grainstone lithofacies (RBP and CAP/G lithofacies) across the Ras ir Raheb (low displacement) and Victoria Lines (high displacement) fault zones.

Cataclasis, which is only observed within discontinuous lenses, up to 0.5 m in thickness on the PSS in the high displacement fault zone, causes the collapse of macro and meso porosity (Figures 10 a and 14 b). This reduction in macro and meso porosity significantly reduces permeability (relative to the protolithology) to a minimum of 0.0001mD.

5.3.2 Micrite Supported Lithofacies

In the micrite supported lithofacies, fracturing and brecciation are expected to enhance the permeability (Nelson, 1985) throughout the WDDZ, fracture splay zone and fault core in both

the low and high displacement fault zones (Figure 17 a), however, the precise permeability increases are unquantified.

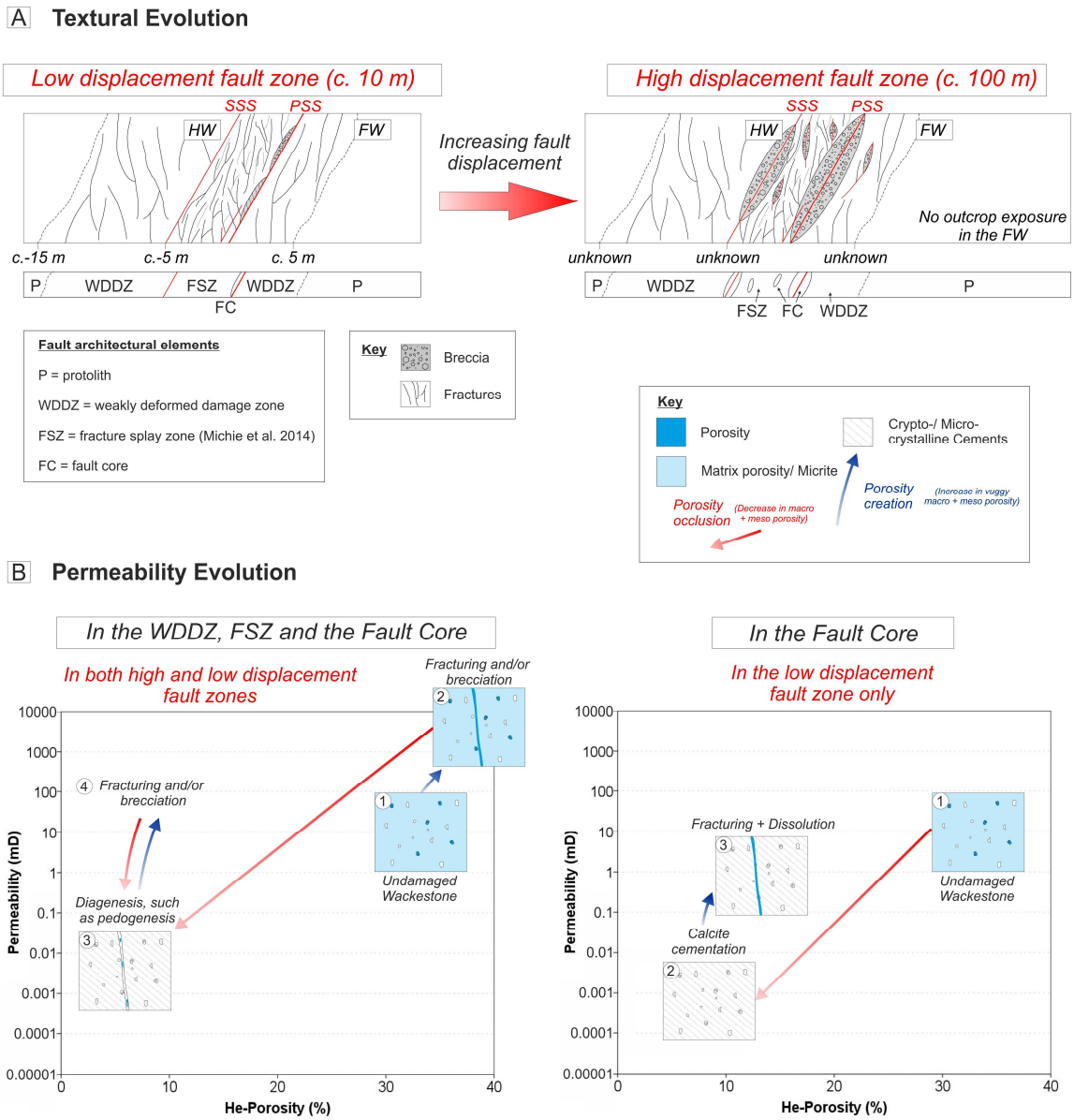

Figure 17 - Spatial and temporal evolution of A) textures and B) porosity and permeability in the wackestone lithofacies (PFW lithofacies) across the Ras ir Raheb (low displacement) and Victoria Lines (high displacement) fault zones.

In the low displacement fault zone, localised calcite cemented lenses are observed on the PSS. This cementation reduces the permeability by occluding the macro and meso porosity (Figure 8), however, subsequent fracturing has enhanced the permeability to a minimum of

0.01mD (Figure 17 b). Similar to the grain supported lithofacies, the diagenetic potential of the micrite supported lithofacies is increased as a result of fracturing and brecciation. In the low displacement fault zone, this enhanced diagenetic potential does not, however, lead to any significant diagenetic modifications. On the contrary, in the high displacement fault zone pedogenesis, including the pervasive replacement of precursor textures by calcite cements (Figure 13 b, c and d), is promoted due to this enhanced potential within a meteoric environment.

Pedogenesis significantly occludes the macro and meso porosity and creates small quantities of isolated mouldic porosity (Figure 14), causing permeability to decrease to a minimum of 0.001mD (Figure 17 b). Although fracturing following the pedogenesis can enhance the permeability, the resultant increase in diagenetic potential often permits further diagenetic alterations, including additional pedogenesis, as well as veining and aggrading neomorphism, which occlude the fractures causing the permeability to decrease back to 0.001mD (Figure 17 b). This trend in permeability associated with fracturing is likely to be episodic, as indicated by cross-cutting fractures and crack-seal textures in the veins (Figure 13 e).

5.4 Permeability Architecture

The temporal and spatial evolution of permeability provides the basis to predict the *in situ* distribution of permeability (i.e. permeability architecture) across fault zones in the subsurface. Caine et al. (1996) devise a conceptual scheme that relates the architecture of a fault zone to its fluid flow. According to this scheme, combined conduit-barrier fault zone architectures are composed of a fault core that is dominated by fault lithologies, such as cataclasites, surrounded by a damage zone, which is composed of abundant subsidiary slip surfaces and fractures. The fault core acts as barrier to fluid flow, whereas the damage zone acts as a fluid flow conduit (Caine et al., 1996). The conduit-barrier fault zone architecture of

Caine et al. (1996) is used to explain permeability trends in several carbonate hosted normal fault zones (Agosta et al., 2012, 2010, 2007; Billi et al., 2003; Matonti et al., 2012; Micarelli et al., 2006) and can also be applied to the studied normal fault zones of the Maltese Islands.

Independent of lithofacies and fault displacement, the damage zones (WDDZ and fracture splay zone) act as conduits for fluid flow as a result of the development of fracture and vuggy pore systems. However, during the early stages of fault development, the damage zones in the grain supported lithofacies were composed of dense neomorphic cement (Figure 12 a and b). As a result of this cement, the damage zones hosted low porosity and hence low permeability, and hence are likely to have acted as baffles to across fault fluid flow. Therefore, the documented textural changes suggest that the permeability architecture of normal fault zones changes through time.

The fault cores are composed of breccias and cataclasites, which are associated with very low permeability values (0.001-0.0001mD) due to the collapse of porosity associated with cataclasis and porosity occlusion related to diagenetic alterations following brecciation. The cataclasites, breccias and associated diagenetically altered fault rocks are commonly fractured (Figures 7 f and 10 c) and have a discontinuous distribution. Matonti et al. (2012) document discontinuous fractured zones along the PSS of a carbonate hosted fault zone and consequently suggest that the fluid flow across the PSS is likely. Similarly in this study, as a result of the fracturing and discontinuous distribution of fault lithologies, the fault core is expected to act as a baffle to across fault fluid flow rather than a seal. However, the extent of the fault lithologies increases with fault displacement suggesting that the baffling effect increases with higher displacement.

6 Conclusions

Contrasting lithofacies in the same fault zones undergo different fault damage and fault related diagenetic processes. The fault related processes also vary according to fault displacement. The spatial and temporal evolution of permeability across the fault zones is controlled by these processes.

Aggrading neomorphism is observed in the grain supported lithofacies (packstones and pack-grainstones) throughout the damage zone associated with the high (*c*. 100 m) and low (*c*. 10 m) displacement fault zones. This process pervasively occludes the primary pore volume, particularly macro and meso pores, and reduces the permeability to a minimum of 0.0001mD. Aggrading neomorphism is active within the grain supported lithofacies only due to the metastability of the allochems comprising these lithofacies, while in the micrite supported lithofacies (wackestones), it is inhibited due to the clay content in the matrix and relatively stable mineralogical composition of the allochems. Fracturing is the first fault related process that affects the micrite supported lithofacies, while in the grain supported lithofacies, fracturing postdates the aggrading neomorphism. The fracturing is observed throughout the damage zones and is expected to increase permeability. The low porosity and cemented textures in the grain supported lithofacies, which result from aggrading neomorphism, promote fracturing. Conversely, in the micrite supported lithofacies fracturing is promoted by the homogeneous texture, the absence of significant mechanical heterogeneities and the small quantities of cement. The fractured lithologies have an enhanced diagenetic potential due to their improved permeabilities, leading to a variety of diagenetic modifications, such as dissolution and pedogenesis. Dissolution further enhances permeability by creating vuggy macro and meso pores, while pedogenesis can pervasive occlude the primary porosity resulting in decreases in permeability to a minimum of 0.001mD.

In the fault core, the fractures in the grain and micrite supported lithofacies develop into breccias by means of hydraulic brecciation due to increasing shear stresses and pore

pressures. The breccias form discontinuous lenses along slip surfaces and display a wider development in the high displacement fault zone. Likewise with the fractured lithologies in the damage zone, brecciation enhances the diagenetic potential of the rocks, promoting dissolution and pedogenesis. Therefore the permeability evolution of the breccias in the fault core is comparable to fractured lithologies in the damage zones. Cataclasis of the grain supported lithofacies is observed within discontinuous lenses along the PSS in the high displacement fault zone only. This process causes the collapse of the primary pore system, leading to a decrease in permeability to a minimum of 0.0001mD. Minor and episodic fracturing is observed within the fault core breccias and cataclasites. This fracturing, coupled with the discontinuous distribution of the fault lithologies is likely to permit fluid flow across the fault cores to a degree.

Despite the differing evolutionary pathways of the contrasting lithofacies, the fault zones, independent of displacement, display a conduit-baffle permeability architecture; the damage zones are fluid flow conduits, while the fault cores are baffles to across fault flow. However, the permeability architecture is expected to vary through time due to the evolution of fault related textures with displacement.

7 Acknowledgements

The authors would like to thank Total E&P and BG Group for project funding and support, and the Industry Technology Facilitator for facilitating the collaborative development (grant number 3322PSD). The authors would also like to express their gratitude to the Aberdeen Formation Evaluation Society and the College of Physical Sciences at the University of Aberdeen for partial financial support. Raymi Castilla (Total E&P), Fabrizio Agosta, Cathy Hollis and Piero Gianolla are also thanked for their constructive comments and suggestions to improve the standard of this manuscript as are John Still and Colin Taylor (University of Aberdeen) for technical assistance in the laboratory.

References

Agosta, F., Alessandroni, M., Antonellini, M., Tondi, E., Giorgioni, M., 2010. From fractures to flow: A field-based quantitative analysis of an outcropping carbonate reservoir. Tectonophysics 490, 197–213.

Agosta, F., Aydin, A., 2006. Architecture and deformation mechanism of a basin-bounding normal fault in Mesozoic platform carbonates, central Italy. J. Struct. Geol. 28, 1445–1467.

Agosta, F., Prasad, M., Aydin, A., 2007. Physical properties of carbonate fault rocks, Fucino basin (Central Italy): implications for fault seal in platform carbonates. Geofluids 7, 19–32.

Agosta, F., Ruano, P., Rustichelli, A., Tondi, E., Galindo-Zaldívar, J., Sanz de Galdeano, C., 2012. Inner structure and deformation mechanisms of normal faults in conglomerates and carbonate grainstones (Granada Basin, Betic Cordillera, Spain): Inferences on fault permeability. J. Struct. Geol. 45, 4–20.

Anselmetti, F.S., Eberli, G.P., 1999. The Velocity-Deviation Log : A Tool to Predict Pore Type and Permeability Trends in Carbonate Drill Holes from Sonic and Porosity or Density Logs. Am. Assoc. Pet. Geol. Bull. 83, 450–466.

Anselmetti, F.S., Luthi, S., Eberli, G.P., 1998. Quantitative Characterization of Carbonate Pore Systems by Digital Image Analysis. Am. Assoc. Pet. Geol. Bull. 82, 1815–1836.

Arakel, A. V, 1982. Genesis of Calcrete in Quaternary Soil Profiles, Hutt and Leeman Lagoons, Western Australia. J. Sediment. Res. 52, 109–125.

Bastesen, E., Braathen, A., 2010. Extensional faults in fine grained carbonates – analysis of fault core lithology and thickness–displacement relationships. J. Struct. Geol. 32, 1609–1628.

Bathurst, R.G.C., 1975. Carbonate sediments and their diagenesis. Elsevier.

Bausch, W.M., 1968. Clay content and calcite crystal size of limestones. Sedimentology 10, 71–75.

Billi, A., Salvini, F., Storti, F., 2003. The damage zone-fault core transition in carbonate rocks: implications for fault growth, structure and permeability. J. Struct. Geol. 25, 1779–1794.

Bons, P.D., Elburg, M.A., Gomez-Rivas, E., 2012. A review of the formation of tectonic veins and their microstructures. J. Struct. Geol. 43, 33–62.

Bonson, C.G., Childs, C., Walsh, J.J., Schöpfer, M.P.J., Carboni, V., 2007. Geometric and kinematic controls on the internal structure of a large normal fault in massive limestones: The Maghlaq Fault, Malta. J. Struct. Geol. 29, 336–354.

Budd, D.A., 2002. The Relative Roles of Compaction and Early Cementation in the

Destruction of Permeability in Carbonate Grainstones: A Case Study from the Paleogene of West-Central Florida, USA. J. Sediment. Res. 72, 116–128.

Buxton, M.W.N., Pedley, H.M., 1989. A standardized model for Tethyan Tertiary carbonate ramps. J. Geol. Soc. London. 146, 746–748.

Caine, J.S., Evans, J.P., Forster, C.B., 1996. Fault zone architecture and permeability structure. Geology 24, 1025–1028.

Caron, V., Nelson, C.S., 2009. Diversity of Neomorphic Fabrics in New Zealand Plio-Pleistocene Cool-Water Limestones: Insights into Aragonite Alteration Pathways and Controls. J. Sediment. Res. 79, 226–246.

Carrio-Schaffhauser, E., Gaviglio, P., 1990. Pressure solution and cementation stimulated by faulting in limestones. J. Struct. Geol. 12, 987–994.

Chester, F.M., Logan, J.M., 1986. Implications for mechanical properties of brittle faults from observations of the Punchbowl fault zone, California. Pure Appl. Geophys. 124, 79–106.

Chester, F.M., Logan, J.M., 1987. Composite planar fabric of gouge from the Punchbowi Fault, California. J. Struct. Geol. 9, 621–634.

Choquette, P.W., Pray, L.C., 1970. Geologic Nomenclature and Classification of Porosity in Sedimentary Carbonates. Am. Assoc. Pet. Geol. Bull. 54, 207–250.

Civile, D., Lodolo, E., Accettella, D., Geletti, R., Ben-Avraham, Z., Deponte, M., Facchin, L., Ramella, R., Romeo, R., 2010. The Pantelleria graben (Sicily Channel, Central Mediterranean): An example of intraplate “passive” rift. Tectonophysics 490, 173–183. doi:10.1016/j.tecto.2010.05.008

Corbett, K., Friedman, M., Spang, J., 1987. Fracture Development and Mechanical Stratigraphy of Austin Chalk , Texas. Am. Assoc. Pet. Geol. Bull. 71, 17–28.

Dart, C.J., Bosence, D.W.J., McClay, K.R., 1993. Stratigraphy and structure of the Maltese graben system. J. Geol. Soc. London. 150, 1153–1166.

Dorobek, S.L., 1987. Petrography, Geochemistry, and Origin of Burial Diagenetic Facies, Siluro-Devonian Helderberg Group (Carbonate Rocks), Central Appalachians. Am. Assoc. Pet. Geol. Bull. 71, 492–514.

Ehrenberg, S.N., 2007. Whole core versus plugs: Scale dependence of porosity and permeability measurements in platform carbonates. Am. Assoc. Pet. Geol. Bull. 91, 835–846.

Ehrlich, R., Crabtree, S.J., Horkowitz, K.O., Horkowitz, J.P., 1991. Petrography and Reservoir Physics 1: Objective Classification of Reservoir Porosity. Am. Assoc. Pet. Geol. Bull. 75, 1547–1562.

Engelder, J.T., 1974. Cataclasis and the Generation of Fault Gouge. Geol. Soc. Am. Bull. 85,

1515–1522. doi:10.1130/0016-7606(1974)85<1515

Etheridge, M.A., Wilkie, J.C., 1979. Grainsize reduction, grain boundary the flow strength of mylonites sliding and. Tectonophysics 58, 159–178.

Evans, J.P., 1990. Thickness-displacement relationships for fault zones. J. Struct. Geol. 12, 1061–1065.

Fossen, H., Schulz, R.A., Shipton, Z.K., Mair, K., 2007. Deformation bands in sandstone : a review. J. Geol. Soc. London. 164, 755–769.

Gatt, P.A., 2012. Carbonate Facies, Depositional Sequences and Tectonostratigraphy of the Palaeogene Malta Platform. University of Durham.

Gaviglio, P., Vandycke, S., Schroeder, C., Coulon, M., Bergerat, F., Dubois, C., Pointeau, I., 1999. Matrix strains along normal fault planes in the Campanian White Chalk of Belgium: structural consequences. Tectonophysics 309, 41–56.

Groshong, R.H., 1988. Low-temperature deformation mechanisms and their interpretation. Geol. Soc. Am. Bull. 100, 1329–1360. doi:10.1130/0016-7606(1988)100<1329

Haines, T.J., Neilson, J.E., Healy, D., Michie, E.A.H., Aplin, A.C., 2015. The impact of carbonate texture on the quantification of total porosity by image analysis. Comput. Geosci. 85, 112–125. doi:10.1016/j.cageo.2015.08.016

Hollis, C., Vahrenkamp, V., Tull, S., Mookerjee, A., Taberner, C., Huang, Y., 2010. Pore system characterisation in heterogeneous carbonates: An alternative approach to widely-used rock-typing methodologies. Mar. Pet. Geol. 27, 772–793.

Hood, S.D., Nelson, C.S., 1996. Cementation scenarios for New Zealand Cenozoic nontropical limestones. New Zeal. J. Geol. Geophys. 39, 109–122.

Klinkenberg, L.J., 1941. The permeability of porous media to liquids and gases. Drill. Prod. Pract. 200–213.

Knipe, R.J., 1989. Deformation mechanisms - recognition from natural tectonites. J. Struct. Geol. 11, 127–146.

Knoerich, A.C., Mutti, M., 2006. Missing Aragonitic Biota and the Diagenetic Evolution of Heterozoan Carbonates: A Case Study from the Oligo-Miocene of the Central Mediterranean. J. Sediment. Res. 76, 871–888.

Larsen, B., Grunnaleite, I., Gudmundsson, A., 2010. How fracture systems affect permeability development in shallow-water carbonate rocks: An example from the Gargano Peninsula, Italy. J. Struct. Geol. 32, 1212–1230.

Lavenu, A.P.C., Lamarche, J., Salardon, R., Gallois, A., Marié, L., Gauthier, B.D.M., 2014. Relating background fractures to diagenesis and rock physical properties in a platform–slope transect. Example of the Maiella Mountain (central Italy). Mar. Pet. Geol. 51, 2–19. doi:10.1016/j.marpetgeo.2013.11.012

Lønøy, A., 2006. Making sense of carbonate pore systems. Am. Assoc. Pet. Geol. Bull. 90, 1381–1405.

Loucks, R.G., 2002. Controls on Reservoir Quality in Platform-Interior Limestones Around the Gulf of Mexico : Example from the Lower Cretaceous Pearsall Formation in South Texas Depositional Setting and Systems of the Pearsall Formation. Gulf Coast Assoc. Geol. Soc. Trans. 52, 659–672.

Lucia, F.J., 1983. Petrophysical Parameters Estimated From Visual Descriptions of Carbonate Rocks: A Field Classification of Carbonate Pore Space. J. Pet. Technol. 35, 629–637.

Lucia, F.J., 1995. Rock-Fabric/Petrophysical Classification of Carbonate Pore Space for Reservoir Characterization. Am. Assoc. Pet. Geol. Bull. 79, 1275–1300.

Maliva, R.G., Dickson, J.A.D., 1992. The mechanism of skeletal aragonite neomorphism: evidence from neomorphosed mollusks from the upper Purbeck Formation (Late Jurassic-Early Cretaceous), southern England. Sediment. Geol. 76, 221–232.

Matonti, C., Lamarche, J., Guglielmi, Y., Marié, L., 2012. Structural and petrophysical characterization of mixed conduit/seal fault zones in carbonates: Example from the Castellas fault (SE France). J. Struct. Geol. 39, 103–121.

Mauldon, M., Dunne, W.M., Jr, M.B.R., 2001. Circular scanlines and circular windows : new tools for characterizing the geometry of fracture traces. J. Struct. Geol. 23, 247–258.

Melim, L.A., Anselmetti, F.S., Eberli, G.P., 2001. The Importance of Pore Type on Permeability of Neogene Carbonates, Great Bahama Bank, in: Subsurface Geology of a Prograding Carbonate Platform Margin Great Bahama Bank Results of the Bahamas Drilling Project. SEPM Special Publication, pp. 217–238.

Micarelli, L., Benedicto, A., Wibberley, C.A.J., 2006. Structural evolution and permeability of normal fault zones in highly porous carbonate rocks. J. Struct. Geol. 28, 1214–1227.

Michie, E.A.H., 2015. Influence of host lithofacies on fault rock variation in carbonate fault zones: A case study from the Island of Malta. J. Struct. Geol. 76, 61–79. doi:10.1016/j.jsg.2015.04.005

Michie, E.A.H., Haines, T.J., Healy, D., Neilson, J.E., Timms, N.E., Wibberley, C.A.J., 2014. Influence of carbonate facies on fault zone architecture. J. Struct. Geol. 65, 82–99. doi:10.1016/j.jsg.2014.04.007

Mitchell, T.M., Faulkner, D.R., 2009. The nature and origin of off-fault damage surrounding strike-slip fault zones with a wide range of displacements: A field study from the Atacama fault system, northern Chile. J. Struct. Geol. 31, 802–816.

Nelson, R.A., 1985. Geologic Analysis of Naturally Fractured Reservoirs.

Pedley, H.M., 1978. A new lithostratigraphical and palaeoenvironmental interpretation for

the coralline limestone formations of the Maltese Islands (Miocene). Overseas Geol. Miner. Resour. 54, 273–291.

Pedley, H.M., House, M.R., Waugh, B., 1976. The geology of Malta and Gozo. Proc. Geol. Assoc. 87, 325–341.

Petracchini, L., Antonellini, M., Billi, A., Scrocca, D., 2012. Fault development through fractured pelagic carbonates of the Cingoli anticline, Italy: Possible analog for subsurface fluid-conductive fractures. J. Struct. Geol. 45, 21–37. doi:10.1016/j.jsg.2012.05.007

Rasband, W.S., 2014. ImageJ. http://imagej.nih.gov/ij/.

Rath, A., Exner, U., Tschegg, C., Grasemann, B., Laner, R., Draganits, E., 2011. Diagenetic control of deformation mechanisms in deformation bands in a carbonate grainstone. Am. Assoc. Pet. Geol. Bull. 95, 1369–1381.

Scholle, P.A., Ulmer-Scholle, D.S., 2003. A color guide to the petrography of carbonate rocks: grains, textures, porosity, diagenesis. AAPG Memoir 77.

Shipton, Z.K., Soden, A.M., Kirkpatrick, J.D., Bright, A.M., Lunn, R.J., 2006. How Thick is a Fault ? Fault Displacement-Thickness Scaling Revisited, in: Abercrombie, R., McGarr, A., Di Toro, G., Kanamori, H. (Eds.), Radiated Energy and the Physics of Faulting. American Geophysical Union Monograph Series 170, pp. 193–198.

Sibson, R.H., 1977. Fault rocks and fault mechanisms. J. Geol. Soc. London. 133, 191–213.

Sibson, R.H., 1986. Brecciation processes in fault zones: Inferences from earthquake rupturing. Pure Appl. Geophys. 124, 159–175.

Solymar, M., Fabricius, I.L., 1999. Image analysis and estimation of porosity and permeability of Arnager Greensand, Upper Cretaceous, Denmark. Phys. Chem. Earth, Part A Solid Earth Geod. 24, 587–591.

Storti, F., Billi, A., Salvini, F., 2003. Particle size distributions in natural carbonate fault rocks: insights for non-self-similar cataclasis. Earth Planet. Sci. Lett. 206, 173–186.

Tanikawa, W., Shimamoto, T., 2006. Klinkenberg effect for gas permeability and its comparison to water permeability for porous sedimentary rocks. Hydrol. Earth Syst. Sci. Discuss. 3, 1315–1338.

Tarasewicz, J.P.T., Woodcock, N.H., Dickson, J.A.D., 2005. Carbonate dilation breccias: Examples from the damage zone to the Dent Fault, northwest England. Geol. Soc. Am. Bull. 117, 736–745. doi:10.1130/B25568.1

Tondi, E., 2007. Nucleation, development and petrophysical properties of faults in carbonate grainstones: Evidence from the San Vito Lo Capo peninsula (Sicily, Italy). J. Struct. Geol. 29, 614–628.

Tucker, M., Graham, J., McManus, J., Miller, J., Harwood, G., Hardy, R., Trewin, N.,

Fairchild, I., Hendry, G., Quest, M., 1988. Techniques in Sedimentology.

Tucker, M., Wright, V.P., Dickson, J.A.D., 1990. Carbonate Sedimentology. Blackwell Science.

Underhill, J.R., Woodcock, N.H., 1987. Faulting mechanisms in high-porosity sandstones: New Red Sandstone, Arran, Scotland. Geol. Soc. London, Spec. Publ. 29, 91–105. doi:10.1144/GSL.SP.1987.029.01.09

Vajdova, V., 2004. Compaction, dilatancy, and failure in porous carbonate rocks. J. Geophys. Res. 109, B05204. doi:10.1029/2003JB002508

van der Land, C., Wood, R., Wu, K., van Dijke, M.I.J., Jiang, Z., Corbett, P.W.M., Couples, G., 2013. Modelling the permeability evolution of carbonate rocks. Mar. Pet. Geol. 48, 1–7.

Vik, B., Bastesen, E., Skauge, A., 2013. Evaluation of representative elementary volume for a vuggy carbonate rock—Part: Porosity, permeability, and dispersivity. J. Pet. Sci. Eng. 112, 36–47.

Weger, R.J., Eberli, G.P., Baechle, G.T., Massaferro, J.L., Sun, Y.-F., 2009. Quantification of pore structure and its effect on sonic velocity and permeability in carbonates. Am. Assoc. Pet. Geol. Bull. 93, 1297–1317.

Woodcock, N.H., Mort, K., 2008. Classification of fault breccias and related fault rocks. Geol. Mag. 145, 435–440.

Zhang, J., Wong, T.-F., Davis, D., 1990. Micromechanics of pressure-induced grain crushing in porous rocks. J. Geophys. Res. Solid Earth 95, 341–352.

Highlights

- Two categories of fault processes are active in carbonate hosted fault zones.
- Porosity occlusion processes, e.g. aggrading neomorphism, reduce permeability.
- Porosity creation processes, e.g. fracturing and dissolution, enhance permeability.
- The processes active are dependent on the lithofacies and the fault displacement.
- These processes control the spatial and temporal evolution of permeability.